

# **Evidence for carbon dioxide removal via enhanced rock weathering with steel slag, though not basalt, in a midwestern U.S. field trial**

Daniel P. Maxbauer<sup>1\*</sup>, Ella Milliken<sup>2</sup>, Jahmaine Renzo Yambing<sup>3,4</sup>, Emma Watson<sup>1</sup>, Rachel B. Gregg<sup>1</sup>, Liza Swanson<sup>1</sup>, Jaeun Sohng<sup>5</sup>, Noah W. Sokol<sup>6</sup>, Noah J. Planavsky<sup>2,7</sup>

<sup>1</sup>Geology Department, Carleton College, Northfield, MN, 55057

<sup>2</sup>Department of Earth and Planetary Sciences, Yale University, New Haven, CT, 06511

<sup>3</sup>Department of Earth and Planetary Sciences, Massachusetts Institute of Technology, Cambridge, MA, 02139

<sup>4</sup>Department of Geology and Geophysics, Woods Hole Oceanographic Institution, Woods Hole, MA, 02543

<sup>5</sup>Institute of the Environment, University of California, Davis, CA, 95616

<sup>6</sup>Physical and Life Sciences Directorate, Lawrence Livermore National Laboratory, Livermore, CA, 94550

<sup>7</sup>Yale Center for Natural Carbon Capture, Yale University, New Haven, CT, 06511

\*Corresponding author: [dmaxbauer@carleton.edu](mailto:dmaxbauer@carleton.edu)

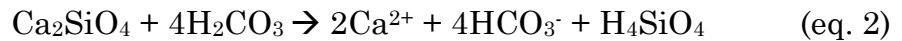
**Keywords:** enhanced weathering, carbon dioxide removal, basalt, steel slag, soil carbon

## **Abstract**

Enhanced weathering is an emergent pathway for permanent atmospheric carbon dioxide removal (CDR). However, despite a dramatic increase in academic and commercial research, there remain relatively few published examples of field evidence demonstrating the effectiveness of enhanced weathering. Here, we present results from a three-year field trial that evaluated steel slag and crushed basalt applied as amendments in a conventional agricultural system in the Midwestern United States. Steel slag applied to initially acidic soil increased porewater pH and alkalinity and increased soil pH and Ca-saturation. Together, changes in porewater chemistry and soil properties provide strong evidence for steel slag weathering and CDR. However, steel slag applied to soils with a neutral initial pH did not generate significant changes in soil or porewater chemistry. In addition, coarse-grained crushed basalt did not generate detectable signals for carbonic acid weathering in any of the soils. However, the impacts of strong acids on mineral weathering were apparent in all three years of monitoring soil porewater chemistry. Overall, the results of this study demonstrate clear evidence for CDR from applying steel slag amendments to cropland soils while highlighting the difficulty of greenhouse gas reduction accounting from enhanced weathering and the variable outcomes that can occur depending on feedstock and soil type.

## 1. Introduction

Enhanced weathering is a promising carbon dioxide removal (CDR) strategy with potential to reach gigaton scale targets within the next decade if widely deployed, while also having potential co-benefits for crop yields and soil health<sup>1-3</sup>. In its simplest form, enhanced rock weathering delivers CDR through the neutralization of carbonic acid, which forms as CO<sub>2</sub> from the atmosphere or soil dissolves into soil waters. The reactions below illustrate both carbonic acid formation (eq. 1) and the neutralization of carbonic acid through reaction with an example Ca-silicate (here, larnite – Ca<sub>2</sub>SiO<sub>4</sub>; eq. 2).



In this simplified case, silicate minerals buffer and consume carbonic acid, release base cations (here Ca<sup>2+</sup> but commonly Mg<sup>2+</sup> as well), and convert the dissolved carbon into bicarbonate (HCO<sub>3</sub><sup>-</sup>), increasing the alkalinity of the soil porewaters. The bicarbonate and base cations generated through enhanced rock weathering eventually leach through the soil profile and into river networks to reach the ocean. There, bicarbonate can persist for thousands of years, or eventually precipitate calcium carbonate, leading to effectively permanent CDR<sup>4-9</sup>.

In croplands, enhanced rock weathering aims to optimize the practice of soil pH management by using materials and deployment strategies designed to maximize CDR, while providing cost effective solutions to farmers with agronomic co-benefits. From the perspective of carbon balance, using silicate rocks for pH management leads to more permanent carbon removal compared to traditional carbonate ag lime amendments, with no risk of releasing the fossil carbon contained in carbonate rocks. In addition, silicate rocks often offer a similar set of co-benefits as ag lime, including the release of micronutrients, increased crop yields, and reduced emissions of other greenhouse gases such as nitrous oxide<sup>9-14</sup>. Most commonly, enhanced weathering studies target natural silicate rocks like basalt<sup>8,10,11</sup>. However, industrial products like steel slag and returned concrete have also drawn attention due to their relatively rapid weathering rates, potential for CDR, and agronomic benefits<sup>15,16,17</sup>.

Despite the potential of enhanced weathering, there are still very limited field studies that have published empirical evidence for rates of rock weathering and CDR. Perhaps the most difficult aspect of enhanced weathering as a CDR approach is the direct measurement of mineral weathering and the accompanying CDR in field deployments<sup>18,19</sup>. Published rates for CDR from enhanced weathering field trials are highly variable, spanning four orders of magnitude<sup>20</sup>. Given that commercial carbon markets and widespread adoption hinge on adequate proof that enhanced weathering is delivering CDR at scale, robust demonstration of the quantity of CDR is essential<sup>3</sup>. In the past several years, work on enhanced weathering has rapidly increased across

academic and industry groups, with a growing emphasis on developing field trials and measurement, reporting, and verification (MRV) techniques across different soil types, climate patterns, and crop regimes<sup>9,10,12,21–24</sup>. Current strategies for measurement in enhanced weathering generally focus on tracking weathering rates through measurement of cation-loss from feedstock material<sup>25,26</sup>, direct sampling and measurement of soil porewater chemistry<sup>24,27</sup>, and local watershed monitoring<sup>21,28</sup>.

The collection and measurement of soil porewaters provides arguably the most direct measure of weathering and initial CDR through analysis of total alkalinity (which approximates the concentration of bicarbonate in most natural waters<sup>21,24,29</sup>), dissolved inorganic carbon, base cations, and non-carbonate system anions. However, porewaters are notoriously difficult to sample, and cannot easily be measured continuously. Watershed scale studies can provide a large-scale integrated measure of CDR, but signals can be dilute and difficult to measure<sup>21</sup>. In addition, weathering products have variable mobility in soil, with products interacting with charged exchange sites on soil particles, or becoming entangled in secondary mineral phases that are difficult to detect<sup>30</sup>. Given some of these complexities, solid-phase cation-loss approaches that leverage soil samples to evaluate the loss of base-cations from applied feedstock material is an emerging proxy<sup>25</sup>. However, mass-balance based approaches are a measure of the rate of chemical weathering and base cation release that establishes a potential rate of CDR<sup>27</sup>. When converting weathering rates to CDR, complications around the transport time of released base cations and potential impacts of strong acid weathering are areas of active research and debate<sup>31,32</sup>.

Limited attention has been paid to any associated positive or negative impacts of crushed rock amendments on soil organic matter (SOM), Earth's largest terrestrial pool of organic C, and a critical source of nitrogen (N) and other nutrients<sup>33,34</sup>. Given that positive effects on SOM may enhance CDR and boost soil fertility, while negative effects could entirely negate any benefit of inorganic CDR this is an essential area for continued work. The limited available evidence shows contrasting effects of crushed rock on SOM pools in different ecosystems, as well as variable effects on different SOM pools including the slower-cycling mineral-associated soil organic matter (MAOM) and faster-cycling particulate organic matter (POM)<sup>34,35,36</sup>. No studies to date have investigated effects on SOM pools in a Midwestern field trial, nor the effects of steel slag on SOM, MAOM, and POM. Put together, there is a clear need for more research and data to inform our collective understanding of enhanced weathering as emerging CDR pathways.

Here, we report results from a three-year enhanced weathering trial in Southeastern Minnesota. We applied crushed basalt and steel slag to a strip-till corn and soybean rotational field typical of a conservation-oriented Midwestern farm. Porewater chemistry, soil properties, and gas fluxes were monitored for three field seasons. We evaluated whether there was direct evidence for mineral weathering and CDR. In

addition, we evaluated the role of strong acid weathering and considered the impacts of strong acids on CDR quantification. Finally, we investigated how weathering of crushed basalt and steel slag affected soil organic carbon cycling, through monitoring soil CO<sub>2</sub> gas-flux, total SOM, and different soil organic carbon pools (MAOM and POM).

## 2. Site Details and Experimental Methods

### 2.1 Field Site

The field trial is situated on an eight-hectare agricultural field on the campus of Carleton College in Northfield, Minnesota (Figure 1). Since the 1930s, the field has been in near-constant cultivation, with corn and soybeans rotating as the primary crops for the past several decades. In the mid 2010s the field transitioned from conventional tillage to strip-tillage. Crop rotation during the field trial included soybeans in 2022 and 2024 and corn in 2023. Aerial images of the site show that there has been land-management variation across the site since at least 2003, with the northern portion of the field remaining out of cultivation in a subset of years (see Supplemental Figure S1). In addition, dredged sediments from an artificial lake on campus were spread across the northern portion of the field during the early 2000s (estimated extent of dredging covers the full extent of Block B and all of Block A except the easternmost slag plot). These variations in land use correspond to a gradient in soil properties across the field area (discussed below in section 3.1), making it ideal to explore the effects of varying soil types on enhanced weathering.



**Figure 1.** Field map and overview of study area. Location is Northfield Minnesota (inset map in upper left), with the study field (outlined in yellow at left) on campus at Carleton College. Detailed plot layout shown at right with basalt, slag, and control treatments distributed across the field in four experimental blocks.

Soils in the region are dominated by loam developed atop Quaternary glacial sediments or Ordovician sedimentary units (limestones, dolostones, and sandstones). In this field, soils are loam and clay loam developed atop Quaternary loess and fine

loamy till mapped primarily as the Hayden loam and Blooming silt loam in the field area<sup>37</sup>. The Hayden loam is a mesic, superactive, Glossic Hapludalf and The Blooming silt loam is a fine-loamy, mixed, superactive mesic Mollic Hapludalf<sup>37</sup>.

Climate in the area is temperate, with a mean annual temperature (MAT) of 7.9°C and mean annual precipitation (MAP) of 902 mm yr<sup>-1</sup> (Supplemental Table S1; NOAA). Growing season climate in the area (May-Sept) has average temperature of 18.5°C and rainfall of 574 mm (1990-2020 normals for Rice County; NOAA). Conditions during the three years of this experiment were generally warmer than normal in 2023 and 2024 and drier than normal in 2022 and 2023 (see Supplemental Table S1).

## **2.2 Experimental Design, Baseline Sampling, and Materials**

We used a randomized block design to distribute treatment and control plots (~0.5 acres each) across the study area to minimize impacts of soil variation on our interpretation of treatment effects (Figure 1). A set of baseline soil samples were collected in June 2021 to constrain soil properties across the field area prior to spreading of any feedstock. Baseline soil was collected at four depth intervals: 0-10 cm, 10-20 cm, 20-40 cm, and 40-60 cm. At each depth interval, a total of 12 individual soil cores were collected at semi-random locations across the plot area (~0.5 acres) and homogenized into one sample per plot (see Supplemental Figure S2). All homogenized baseline samples were air dried and sieved to remove any particles > 2 mm prior to analysis.

Each baseline soil sample was analyzed for soil pH, total soil organic matter (SOM) and SOM pools (MAOM and POM; see methods for this below in section 2.3), carbonate minerals, cation exchange capacity (CEC), and 27 element microwave digestion ICP-OES. Soil pH was measured using a Mettler Toledo Seven-Multi pH meter and InLab Routine Pro electrode on a 1:1 soil to water mixture of 10 g dried soil and 10 mL deionized water with a 15-minute equilibration period. Weight percentage organic matter (SOM) and carbonate minerals were determined through loss-on-ignition (LOI) at temperatures of 360°C and 1000°C respectively, with a 2-hour heating period at each temperature and an intermediate heating at 105°C to remove any residual water. For CEC and the 27 element ICP-OES, baseline samples were sent to the University of Minnesota Research Analytical Laboratory (RAL) in St. Paul, Minnesota, USA. Complete analytical methods for those analyses are available on the RAL website (<https://ral.cfans.umn.edu/tests-analysis/soil-analysis>) but are briefly summarized here. CEC was calculated by summation of the exchangeable cations Ca, Mg, Na, K, and Al through an ammonium acetate extraction and subsequent evaluation of leachate using an ICP-OES. The 27-element analysis involved a microwave digestion in concentrated nitric acid following EPA procedure 3051 and measurement using an ICP-OES. The data for the 27 element ICP-OES analysis is not shown in a figure but is available in the Supplemental Data.

Spreading of feedstock materials was completed in November 2021. Four treatment plots were amended with basalt at a target rate of 10 tonnes acre<sup>-1</sup> and four plots with slag at a target rate of 2 tonnes acre<sup>-1</sup> using commercial ag lime spreading equipment. To validate application rates, six pie pans were placed in each plot at random before spreading (for pan test results and average spreading rates see Supplementary Table S2).

Feedstock used for treatments in this study was basalt and steel slag. The basalt is a commercially available quarry sand product derived from an aggregate quarry in the Chengwatana Volcanics of the Keweenaw Supergroup, a sequence of lavas, tuffs, and interflow sedimentary rocks associated with the Neoproterozoic (~1.1 Ga) failed rifting of the midcontinent<sup>38</sup>. The material is dominantly coarse to medium grained sand (~63% passing 0.5 mm sieve) with 20% fine sand (< 0.25 mm) or finer, placing this on the coarse side of feedstocks used for EW trials. Geochemically, the basalt is 15% Ca + Mg and the mineralogy is dominated by plagioclase, diopside/augite, chlorite, and epidote. The presence of epidote and chlorite is related to low-grade metamorphism associated with hydrothermal fluids<sup>38</sup>. The steel slag used in this study is a Ca-rich byproduct of steel production. The material is ~50% CaO + MgO with mineralogy dominated by Ca and Mg rich silicate, (hydr)oxides, and amorphous phases. Grain size is finer in comparison to the basalt, with most of the steel slag gradation being medium sand (~65% < 0.6 mm) and ~25% being very fine sand to silt (~27.3% < 0.15mm). Both the basalt and steel slag were byproducts of industrial processes.

### **2.3 Soil Sampling and Analysis Years 1-3**

Soil samples were collected each year of the three-year field trial. Various sampling strategies were adopted in later years to constrain effects of the study treatment and deal with background soil variability. Below, sampling strategies are described for each sampling year: 2022, 2023, and 2024. While all soil data is included in the Supplemental Files, we only discuss soil data in detail from the end of the experiment – sampling year 3 (2024). Below, we briefly describe both sampling strategies and conclusions from evaluating soil in the intermediate years of this study.

In October of 2022 (year 1), soil was collected at 0-10 cm and 10-20 cm depth increments for all treatment plots using the same sampling strategy as the baseline soils. These soils were evaluated for soil pH, organic matter, CEC, and the 27 element ICP-OES, all measured at the RAL facility at the University of Minnesota using methods described above.

In 2023 (year 2), soil was collected during October 2023 at a higher resolution in the southern blocks (C and D) of the field area to determine if higher resolution sampling would reveal a clearer picture of treatment effects. Within an experimental plot, 15 sampling points representing a circular area with a 3 m radius (~28.3 m<sup>2</sup> area) were established (see Supplemental Figure S2). At each sampling point, fifteen 0-10 cm

soil cores were collected and homogenized into a single sampling point sample. Soil pH and exchangeable base cations (Ca and Mg) for year 2 soils significantly increased in both properties in the slag treatment relative to both the control and basalt treatments (see Supplemental Figure S3). The basalt treatment was not statistically different from control for either property (Supplemental Figure S3). Given the improved resolution using higher density sampling, this approach was adopted for evaluating soil properties in year 3 of this project.

In year 3 (2024), all plots were sampled from 0-10 cm at 15 sampling points per plot (following scheme outlined above and in Figure S2). Year 3 soils were evaluated for soil organic matter (SOM; weight percentage; based on loss-on-ignition at 360 °C), soil pH (1:1 slurry), a series of extractable elements using the Mehlich 3 extraction including P, K, B, S, Fe, Mn, Cu, Zn, and exchangeable base cations Ca, Mg, K, and Na. Cation exchange capacity (CEC) and base saturation is reported for each sample. Analytical work on all soils from year 3 of this study was conducted by Waypoint Analytical, LLC (Champaign, Illinois, USA).

For baseline soils (2021), year 1 soils (2022), and year 3 soils (2024) we also evaluated effects on different SOM pools: mineral-associated organic matter (MAOM) and particulate organic matter (POM). We separated MAOM and POM pools using a standard physical fractionation method<sup>39,40</sup>. First, 5-g of air-dried soil was weighed into a 50-mL falcon tube, and 30-mL of 5% sodium hexametaphosphate (NaHMP) was added to disperse aggregates. Samples were then vortexed and placed on a shaker table for 16 h at 200 rpm. After shaking, the soil solution was passed through a 53- $\mu\text{m}$  sieve. The < 53- $\mu\text{m}$  fraction (clay + fine silt fraction; defined as MAOM) and the > 53- $\mu\text{m}$  fraction (sand, coarse silt, and large organic matter fragments; defined as POM) were oven-dried to constant mass at 105 °C. Dried samples were finely ground to a powder-like consistency with a mortar and pestle and analyzed on an elemental analyzer (Lawrence Livermore National Laboratory, Livermore, CA).

We determined the trace and major element composition of the mineral-bound phases to constrain cation loss from the soil surface (e.g., a soil mass balance or TiCAT methodology<sup>25</sup>). This approach uses a mass-balanced based mixing model that constrains mineral weathering rates in enhanced weathering feedstocks. As minerals in applied feedstock are weathered, there is a preferential release of mobile base cations relative to immobile elements like titanium. It can be feasible to disentangle the loss of mobile base cations from a soil-feedstock mixture that has weathered relative to initial baseline measurements<sup>25</sup>. All soil and feedstock samples evaluated using this approach were analyzed for isotope dilution inductively coupled mass spectrometry (ID-ICP-MS) at Yale University following methods in Ref <sup>25</sup>.

## 2.4 Porewater chemistry

In each growing season of the study, lysimeters were used to collect shallow (0-20 cm) soil porewater. In 2022, porewater monitoring occurred in each of the 12 experimental plots. Porewater in the northern experimental plots with high initial soil pH (> 7; all of Block B and Block A basalt and control plots) had considerably elevated porewater alkalinity compared to soils with more acidic baseline soil pH, likely due to soil carbonates dissolving (see Supplemental Figure S4). Due to difficulties in acquiring sufficient water for analysis, all additional porewater monitoring was conducted on experimental plots with acidic initial soil pH, which includes all the southern plots in blocks C and D along with the slag-treatment plot in the easternmost portion of Block A (see Figure 1 for plot and block layouts). In addition, a set of lysimeters was placed in the buffer strip area between block C and D to serve as additional porewater control given the lack of replicates for control in acidic soil areas.

Porewater was collected weekly to bi-weekly during a 10-week monitoring period between mid-June and mid-August 2022, 2023, and 2024. In each plot, a minimum of 3 suction cup lysimeters were installed at depths of ~15 cm using a soil slurry. A plastic apron was installed around the surface of the lysimeter soil connection to avoid any direct flow paths of water adjacent to the lysimeters. Following installation, the first round of water collected was discarded to avoid any contamination caused by the installation soil slurry. Dry periods during each collection season created gaps in data due to lack of available water. Collected water was combined for all lysimeters within a single experimental plot and refrigerated immediately after collection. Prior to analysis, all water was filtered using a 0.45  $\mu\text{m}$  filter. For elemental analysis, water samples were spiked to 1% nitric acid for preservation shortly after collection.

Total alkalinity and pH were measured on all samples with sufficient sample volume using a Hach AT1000 automated titration system with hydrochloric acid. Units for total alkalinity were initially reported as mg  $\text{CaCO}_3 \text{ L}^{-1}$ . Reported units here are in milliequivalents (meq)  $\text{L}^{-1}$ . We make the conservative assumption that for samples with pH < 8.3, the total alkalinity is equivalent to the bicarbonate alkalinity<sup>24,29</sup>. In 2023, to mitigate limited sample volumes, we conducted alkalinity titrations on diluted samples. Based on regular measurements of alkalinity in reverse osmosis (RO) water used in dilutions, we calculated the samples total alkalinity assuming linear mixing. Because RO waters used in dilutions had relatively low pH (~6), there likely was a minor consumption of alkalinity in samples that were diluted – however this does not appear to be a large effect. For samples that were diluted, we often were able to measure the same sample 2-3 times and use an average value for reporting. When not diluting it was often not possible to obtain duplicate or triplicate measurements of the same sample because of minimum sample volumes (~50 mL) when using pure samples. In comparing alkalinity data, we evaluate measurements throughout the season rather than overanalyzing any one collection interval in part due to these complications.

Major anions, cations, and metals were evaluated throughout the three seasons of monitoring. In all three summers, all water samples were evaluated for a suite of 27 elements using an ICP-OES at the RAL at the University of Minnesota. Here, we report data from this analysis for Ca and Mg, but all elemental data is included within our supplemental dataset. Notably, across all treatments and monitoring years, there are rarely detectable metals (Cr, Pb, Ni, etc) in soil porewaters (see Supplemental Datafile). In 2022, nitrate was measured using colorimetric methods at the RAL at the University of Minnesota. In 2023 and 2024, a set of major anions, including nitrate, sulfate, phosphate, and chloride were measured using an Aquion Ion Chromatography system from ThermoFischer Scientific.

In 2024, water samples were evaluated for total carbon (TC), total organic carbon (TOC), and total inorganic carbon (TIC) at the RAL at the University of Minnesota as an independent check on dissolved carbon separate from alkalinity. Samples were first measured for TC in an Elementar TOC Select Combustion Analyzer. Following an initial TC measurement, an aliquot of the same sample was acidified to remove inorganic carbon and remeasured to quantify TOC. TIC was quantified by subtraction, where  $TIC = TC - TOC$ .

### ***2.5 Soil CO<sub>2</sub> gas flux***

In each of the first two growing seasons (2022 and 2023), soil gas flux was measured using a combination of instruments, chamber types, and soil collar distributions. In 2022, we measured CO<sub>2</sub> gas flux from soils across the study area using an EGM-5 from PP Systems (Amesbury, Massachusetts, USA). Measurements were conducted weekly to bi-weekly at multiple locations throughout each plot. For each measurement, a survey chamber was sealed gently to either the bare soil or to a pre-installed soil collar (PVC pipe) and CO<sub>2</sub> concentration was monitored in the closed chamber for 90 seconds. The flux of CO<sub>2</sub> was then calculated using the change in temperature, air temperature, pressure, and volume of the chamber using standard methods<sup>41</sup>. In 2023, we measured CO<sub>2</sub> gas flux from soil using both the EGM-5 system and a Gasmeter GT5000 Terra multigas FTIR gas analyzer (Gasmeter Technologies Inc; Vantaa, Finland). Functionally, both instruments measure change in CO<sub>2</sub> concentration in a closed chamber over time. In 2023, all measurements were made on pre-installed soil collars at standard locations across each plot.

## **3. Results**

### ***3.1 Soil Properties***

Baseline soil properties across the different blocks were variable (see Supplemental Figures S5 and S6). Blocks A and B in the northern portion of the field trial had higher soil pH, organic matter, carbonate mineral content, and CEC compared with the southern Blocks C and D (Supplemental Figure S5). One exception to this pattern was the slag treatment plot on the eastern side of Block A (Figure 1) which had soil properties that more closely aligned with Blocks C and D (Supplemental Figure S5).

Comparison between soil from baseline and intermediate sampling years (2022 and 2023) revealed considerable variability (see Supplemental Figure S7 for example with soil pH). Here, we focus on surface soils (0-10 cm) collected at higher sampling density in year 3 (2024; see Supplemental Figure S2). In the more acidic soil in blocks C and D, both soil pH and Ca-saturation were significantly higher for slag treated soils compared against control (Figure 2; p-values < 0.05 for Tukey HSD and ANOVA tests). For soils with more neutral initial pH (blocks A and B), we observed no consistent difference in any soil properties in enhanced weathering plots vs control plots (Figure 2). For acidic soils in blocks C and D, slag treatments showed shifts in soil pH and Ca-saturation relative to baseline (boxplots compared with grey squares in Figure 2; statistical tests made difficult due to variable sampling strategies).

There was no impact of basalt or slag on total SOM ( $p > 0.05$  for Tukey HSD and ANOVA tests; Figure 2). There was also no effect of basalt or slag treatment on the change in MAOM-C ( $\text{mg C g soil}^{-1}$ ;  $p > 0.05$  for Tukey HSD and ANOVA tests) or POM-C ( $\text{mg C g soil}^{-1}$ ;  $p > 0.05$  for Tukey HSD and ANOVA tests) pools relative to baseline for both year 1 (2022) and year 3 (2024) soils (Figure 3).

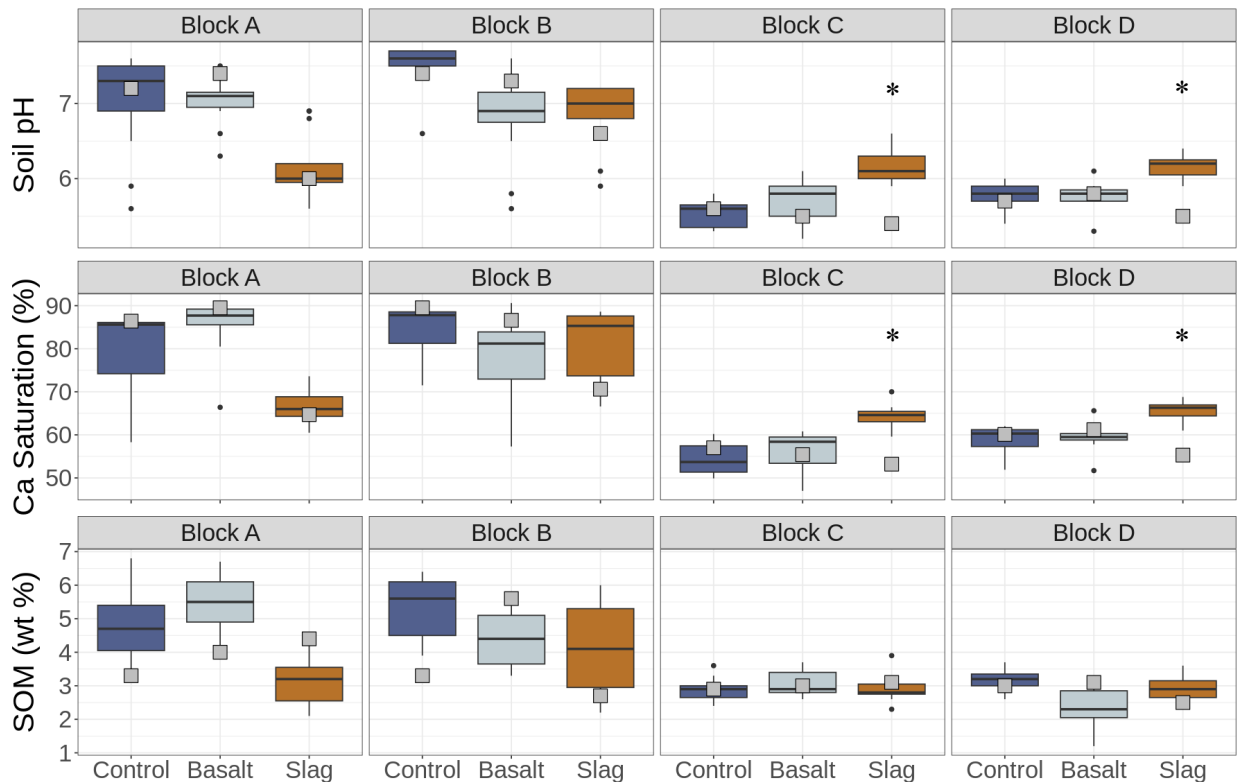


**Figure 2.** Soil properties comparing year 3 (colored boxplots) and baseline (2021; grey squares) soil properties (pH, Ca saturation, and organic matter) across treatments and block. Each boxplot includes  $n = 15$  data points representing the soil sampling points within each plot. Asterisks above boxplots indicate statistically significant differences between control and slag treatment, where p-values < 0.05 for a Tukey HSD and ANOVA test.

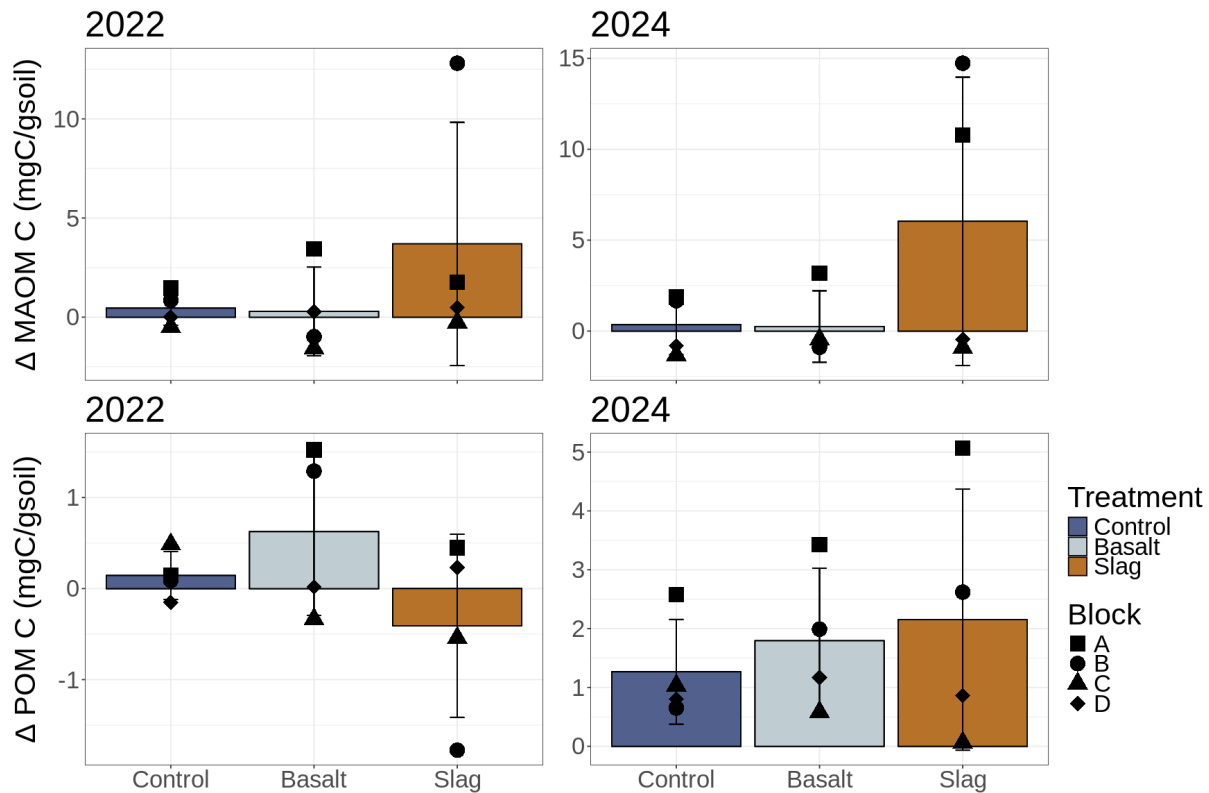


**Figure 3.** Change in mineral associated organic matter ( $\Delta$ MAOM C; upper row) and particulate organic matter ( $\Delta$ POM; lower row) for Year 1 (2022; left column) and Year 3 (2024; right column) relative to baseline (2021). Overall, there were no statistically significant differences by treatment for either year ( $p > 0.05$  with a Tukey HSD and ANOVA tests), though  $\Delta$ MAOM C trended higher in plots A and B in steel slag-amended plots in 2024.

### 3.2 Porewater chemistry

Variation in soil porewater occurred throughout each growing season, in part due to changes in weather (rainfall and temperature), plant activity, and fertilizer applications. In Supplementary Figures S8-S10, major porewater chemical properties including pH, alkalinity, nitrate, and base cations (Ca and Mg) are shown with time for each growing season.

When taken in aggregate across each growing season, porewater pH and alkalinity were significantly elevated in acidic soils treated with steel slag relative to control (Figure 4; all differences are significant at the  $p < 0.05$  level using a Tukey HSD and ANOVA test). There was an increase in Ca and Mg concentrations in slag treated relative to control porewaters in 2022 and 2023, but the difference was not significant in either year ( $p = 0.63$  and  $p = 0.14$  in 2022 and 2023, respectively; see Figure 4). We observed no difference between porewater chemistry in the acidic soils treated with basalt during the 2022 and 2023 growing season, and lysimeters were repurposed in 2024 to focus only on continued monitoring of steel slag treated soil compared to

control soil. There were consistent, measurable concentrations of strong acid anions such as nitrate ( $\text{NO}_3^-$ ) throughout the trial, but there were no significant differences between non-alkaline anion concentrations observed in any of the monitoring years. However, as with calcium and magnesium concentrations, nitrate concentrations in slag treatments in 2023 trended higher than control plots ( $p = 0.2$ ; see Figure 4).

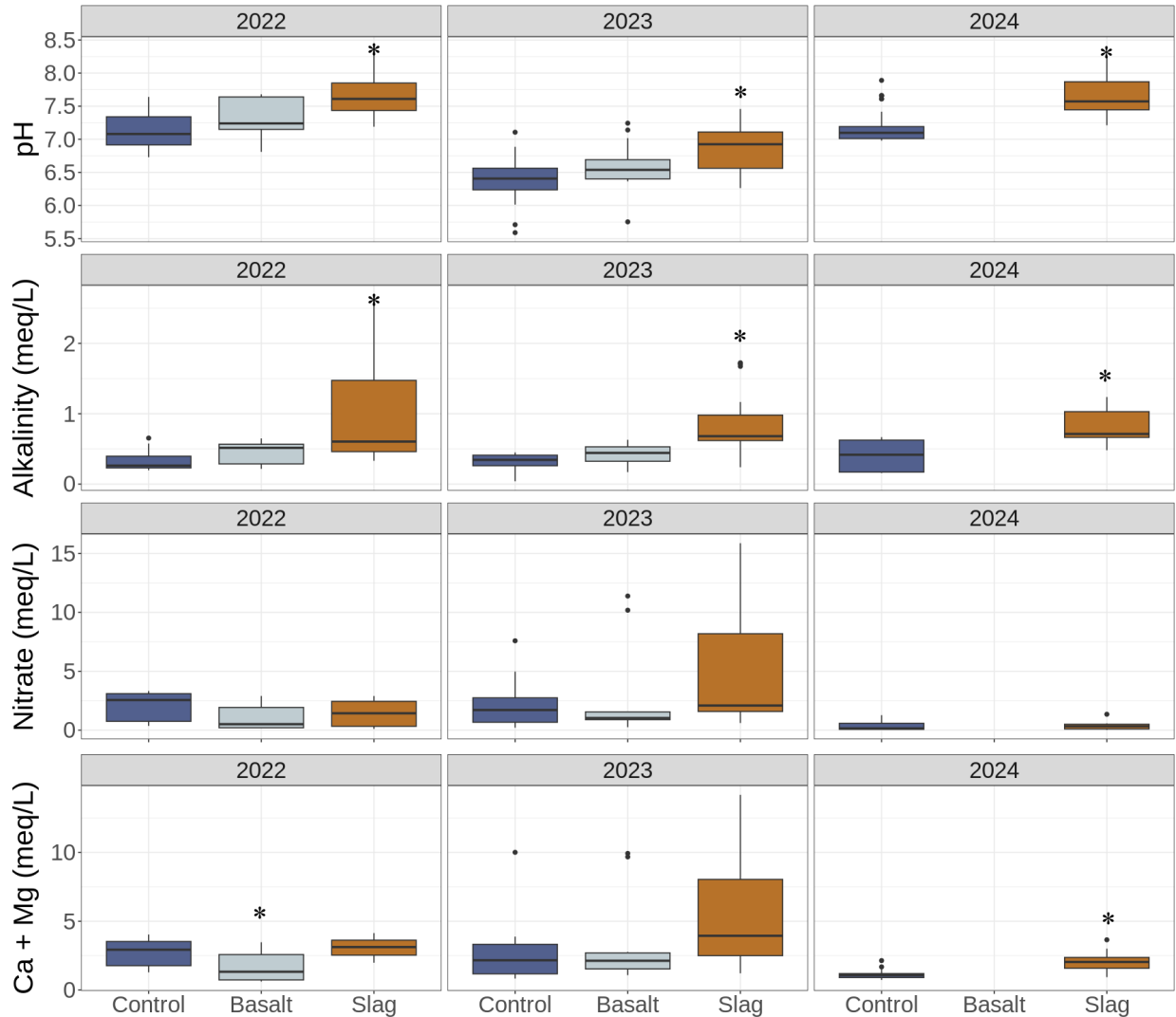


**Figure 4.** Porewater chemistry for acidic soil in southern plots (Blocks C and D). Boxplots represent aggregated data across a summer monitoring season in each indicated sampling year (2022, 2023, and 2024). In 2024 only slag and control plots were monitored due to lack of an observable difference in porewater chemistry between basalt and control during the 2022 and 2023 growing season. Stars indicate statistical significance ( $p < 0.05$ ; Tukey HSD and ANOVA test) between the indicated treatment relative to control. Note that where basalt is significantly different in 2022 in calcium and magnesium concentrations, they are lower than those observed in control, an effect that is opposite that is expected.

In the cases where porewater was measured for heavy metals including Cr, Pb, and Ni, these metals were often below the analytical detection limits (data for Cr, Ni, and Pb are available in the Supplemental File). Ni is the only metal with enough values for statistics, and there was no significant difference with treatment (p-values > 0.05 a Tukey HSD and ANOVA test).

### **3.3 CO<sub>2</sub> Gas Flux**

There was no significant difference in the CO<sub>2</sub> gas flux between basalt-amended or slag-amended soils and control soils when measured using survey chambers with or without soil collars during the 2022 and 2023 monitoring season (p > 0.05 for Tukey HSD and ANOVA test; Supplemental Figure S11).

## **4. Discussion**

Despite an abundance of interest and investment in recent years, there remains relatively limited published data from monitored field deployments. Overall, we found that after three years of monitoring, the steel slag treatment yielded measurable evidence for mineral weathering, decreased acid export, and increased alkalinity export in acidic soils. The effects were less pronounced or not significant in neutral pH soils. The basalt in this study generated small, but not significant, differences relative to untreated controls in all soils. While the outcomes of our study are specific to the feedstocks deployed, the local soil types, and our measurement approach, there are several outcomes that are relevant to enhanced weathering as a CDR strategy more broadly which we discuss below.

### **4.1 Evidence for carbon dioxide removal**

CDR occurs in enhanced weathering through mineral dissolution buffering acidity in soil. In soil porewaters, pH and base cation concentrations should increase as mineral weathering occurs (see eq. 2 above). If carbonic acid is directly buffered, bicarbonate (HCO<sub>3</sub><sup>-</sup>) formation will drive an immediate increase in the alkalinity of the system. In soils amended with steel slag, we observed a significant increase in porewater pH and alkalinity in blocks with acidic soil (Blocks C and D) across three years of monitoring (Figure 4; p < 0.05 for Tukey HSD and ANOVA). While there was an apparent increase in base cation concentration that accompanied the changes in pH and alkalinity, this effect was only significant in 2024 (Figure 4). In addition to soil porewater, soil pH and Ca-saturation for steel slag treatments in Blocks C and D increased significantly in Year 3 (2024) relative to control (Figure 2), providing further support for sustained weathering and CDR over the three-year monitoring period. However, we did not observe significant effects of steel slag in soils with neutral pH (Blocks A and B) nor basalt treatments regardless of initial soil pH (Figures 2 and 4).

In the acidic soils (Blocks C and D), there was consistent evidence for increased pH and increased alkalinity export in steel slag-amended plots, even at a relatively low application rate (2 tonnes acre<sup>-1</sup>) compared to the much higher application rate of crushed basalt (10 tonnes per acre<sup>-1</sup>). This highlights the importance of considering

the reactivity of materials in feedstock selection. Steel slag is composed of calcium and magnesium oxides and hydroxides, Ca-silicates, and Ca-rich amorphous phases that are highly weatherable and alkaline, making it attractive from the perspective of pH management and CDR<sup>15,16,42</sup>. However, steel slag availability in the United States is limited and a large majority of steel slag produced is already utilized within construction markets. Legacy steel slag piles could represent considerable volumes of material but may have more complicated production histories and subsequent potential for heavy metal contamination.

While many studies have focused on basalt as an attractive feedstock for enhanced weathering, the results presented here fail to demonstrate any impact from the applied basalt. This is likely due to the physical and chemical characteristics of the particular basalt used in this study. The grain size of the quarry sand product was likely too coarse-grained to weather measurably in the field over a 3-year period. In addition, the metamorphic minerals epidote and chlorite present in our basalt suggest low-grade metamorphism that may lessen the materials reactivity. In addition, our application rate for basalt (10 tonnes per acre) was relatively low compared to other studies using basalt, and basalt was only applied a single application in the first year, compared to other enhanced weathering deployments with annual applications at higher rates<sup>10,21</sup>. The lower total application volume could have limited our ability to detect a weathering signal. Higher application rates come with agronomic and economic trade-offs, especially considering typical application rates for ag lime are just 0.5-2 tonnes per acre for pH management. Increased trucking costs and soil compaction for spreading large volumes of material, particularly for annual applications, are important considerations. This is an obvious documentation that some fine grained commercially available basalt products will not be suitable for EW deployments. Future work to evaluate new basalt products at finer grain sizes in similar settings should help to determine if weathering signals can be detected at lower application rates with basalt.

There are two plausible explanations for why simple measurements failed to detect impacts from enhanced weathering amendments in soils with neutral pH. First, silicate weathering is pH-sensitive and tends to slow in neutral soils, where lower proton availability reduces mineral dissolution and the release of weathering products. Second, more neutral soils can contain soil carbonates (Supplemental Figure S5) which appear to dominate the soil porewater chemistry (Supplemental Figure S4) and have faster weathering kinetics than silicates. This is consistent with studies monitoring chemical weathering in catchments based on stream water chemistry, where carbonate weathering often predominates the weathering signal. Given the more rapid weatherability of carbonates, they require less rock material to be produced, transported, and spread to achieve a similar buffering effect for soil acidity compared to most silicate feedstocks for enhanced weathering. Prior work that evaluated the carbon removal effects of widespread ag lime usage<sup>43,44</sup>, and more recent work on carbonate-rich returned concrete as a feedstock for enhanced

weathering<sup>17</sup>, both support relatively rapid rates of carbonate weathering that can lead to CDR. Given the requirements of voluntary carbon markets for comparison of project activities against a counterfactual (what would have happened absent the project), quantifying net CDR should consider comparing silicates against carbonates in areas where ag lime use is common (e.g., the Midwest U.S.).

Increased Ca-saturation and soil pH provides direct evidence that steel slag is actively weathering and releasing base cations into the soil environment. Given that Ca-saturation increased (Figure 2), at least a portion of the released calcium is adhering to exchange sites, rather than flushing through the soil column. The timescale and rate at which this calcium will migrate through the soil column is not clear, but will be important for full delivery of CDR<sup>31</sup>. To further quantify rates of cation release and weathering, we applied the Ti-CAT methodology<sup>25</sup>. However, the results were inconclusive using both the high- and low-resolution soil sampling methodologies described above (see section 2.3 and Supplemental Figure S2). This could be due in part to our relatively low application rates, low Ti abundance in steel slag, or lack of high-resolution sampling for baseline soil prior to application for a direct comparison to weathered mixtures. This serves as an example of the importance of high-resolution sampling for soil-based mass balance approaches.

#### ***4.2 Impact on soil CO<sub>2</sub> flux and soil organic matter***

Inorganic CDR that results from mineral weathering may be synergistic with processes that encourage the storage of organic carbon in soils, similar to the relationship between rock weathering and soil organic carbon accrual over long time scales<sup>30</sup>. However, it remains unclear how different feedstocks will interact with organic carbon cycling in different soil types and climates, and on different timescales. Here we evaluate the impacts of enhanced weathering on soil organic carbon cycling by evaluating changes in total SOM, MAOM and POM pools, and monitoring soil CO<sub>2</sub> gas flux from the surface soil.

Both basalt and steel slag did not have any positive or negative effects on total SOM, or MAOM and POM pools (Figures 2 and 3). There was an apparent positive increase in MAOM-C in steel slag-amended treatments in neutral soil (Blocks A and B), but not in acidic soil in southern plots (Blocks C and D; Figure 2). In contrast to most other results where steel slag weathering in more acidic soils in Blocks C and D produce significant results, perhaps steel slag in more neutral soils could have a positive effect on MAOM formation.

Interestingly, while steel slag applied to acidic soils (Blocks C and D) led to significant changes to porewater chemistry that indicates weathering and CDR, the increase in MAOM-C in more neutral soils (Blocks A and B; see Figure 3) treated with steel slag could highlight differing responses of inorganic and organic C pools to enhanced weathering feedstocks based on initial soil pH. In the more neutral soils, slag-derived Ca may have promoted MAOM formation through mechanisms like cation bridging,

aggregate stabilization or by enhancing microbial transformation of organic inputs<sup>45-47</sup>. Even if indicators of weathering in soil porewaters were masked by high background carbonate weathering, Ca released from slag could still interact with native SOM. Additionally, higher initial SOM could support MAOM accrual through organo-organic associations<sup>45,48</sup>. Future work should aim to determine the effects on SOM pools with higher resolution sampling and better replicated trials that vary in soil pH.

Soil CO<sub>2</sub> flux could be influenced by enhanced weathering directly or indirectly. The direct effect of increasing consumption of soil CO<sub>2</sub> through mineral weathering could lead to a decrease in the amount of CO<sub>2</sub> released from the soil surface. In addition, enhanced weathering-induced increases to soil pH may alter soil microbial activity and influence rates of gas flux in soils<sup>48-50</sup>. However, there were no significant differences in CO<sub>2</sub> flux for any treatments in this study. The lack of any significant difference between basalt and steel slag treatments and control plots suggests there are not any significant losses of carbon through increase soil CO<sub>2</sub> flux resulting from enhanced weathering. Although these results are inconclusive, they do not support the hypothesis that mineral addition leads to soil organic carbon loss.

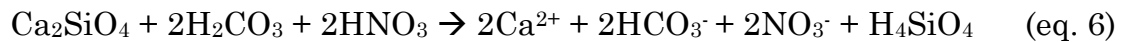
As for any direct impact, the background variability in soil CO<sub>2</sub> flux from biological respiration likely masks any signal from inorganic CDR via enhanced weathering. Diurnal cycles can show variation of ~3-5 μmol CO<sub>2</sub> m<sup>2</sup> s<sup>-1</sup>, or even more. Spatially, there is also considerable variation even within a given area or experimental plot. Even a low-end rate of CO<sub>2</sub> flux in soils from this study of just ~2 μmol CO<sub>2</sub> m<sup>2</sup> s<sup>-1</sup> implies an annual CO<sub>2</sub> flux of ~7.5 tCO<sub>2</sub> acre<sup>-1</sup> yr<sup>-1</sup> being respired out of soils over a frost-free 9-month period. For enhanced weathering amendments to have a chance at being detectable via gas flux measurements, annual rates of carbon removal would need to be perhaps 10-25% of this rate, implying 0.75-1.9 tCO<sub>2</sub> acre<sup>-1</sup> yr<sup>-1</sup>, or higher depending on resolution of measurements. Automated chambers with appropriate spatial resolution and replication could perhaps help to reduce the signal-to-noise issues we encountered here, although existing commercial chambers are expensive and unlikely to be applicable at scale without development of low-cost sensor alternatives. Notably, recent work used an automated array of CO<sub>2</sub> sensors embedded in the soil profile to directly detect decreases in CO<sub>2</sub> flux based on application of basalt in an enhanced weathering trial in Virginia<sup>51</sup>, suggesting this approach could be developed into an effective monitoring strategy.

### ***4.3 Influence of strong acids on weathering***

Soil pH management in agriculture is dominantly a response to the generation of strong acids from the degradation of fertilizers. As an example, ammonia (NH<sub>4</sub><sup>+</sup>), a common ingredient in nitrogen fertilizers, releases acidity during oxidation and forms nitric acid (HNO<sub>3</sub>), which dissociates into acidity (H<sup>+</sup>) and nitrate ions (NO<sub>3</sub><sup>-</sup>) in most soil environments (eq. 3).



Like carbonic acid, strong acids weather silicate minerals and release base cations (eq. 4 below). Instead of achieving charge balance with bicarbonate, strong acid anions (e.g., nitrate,  $\text{NO}_3^-$ ; phosphate,  $\text{PO}_4^{2-}$ ; sulfate,  $\text{SO}_4^{2-}$ ) in porewaters charge balance cations. To illustrate this process, consider the stoichiometric reactions below (eq. 4-6):



Given that carbonic acid neutralization and bicarbonate generation is typically thought of as a key mechanism for delivering CDR in enhanced weathering, strong acid weathering introduces complexity for quantifying CDR in enhanced weathering deployments.

Pure carbonic acid weathering should yield a 1:1 equivalence ratio between base cations and alkalinity (bicarbonate; eq 4), while strong acid weathering will act to increase this ratio by generating an abundance of base cations compared to alkalinity<sup>17,43</sup>. In each year of this study, base cations in soil porewaters exceeded measured alkalinity (see Figure 5). Nonetheless, in all cases, the base cation to alkalinity ratios exceeded 1:1 and in many cases exceeded 2:1 (expected for a mixed acid weathering regime that includes carbonic acid, eq. 6; Figure 5). The apparent effects of strong acid weathering were most pronounced in 2023 when the field was planted with corn, requiring the addition of N-based fertilizers. In 2022 and 2024, the field was planted with soybeans, which do not require additional N-fertilizer. Nitrate in soil porewaters often better aligns with base cation concentration (Figure 5), indicating the importance of N cycling in agricultural soil acid base balances.

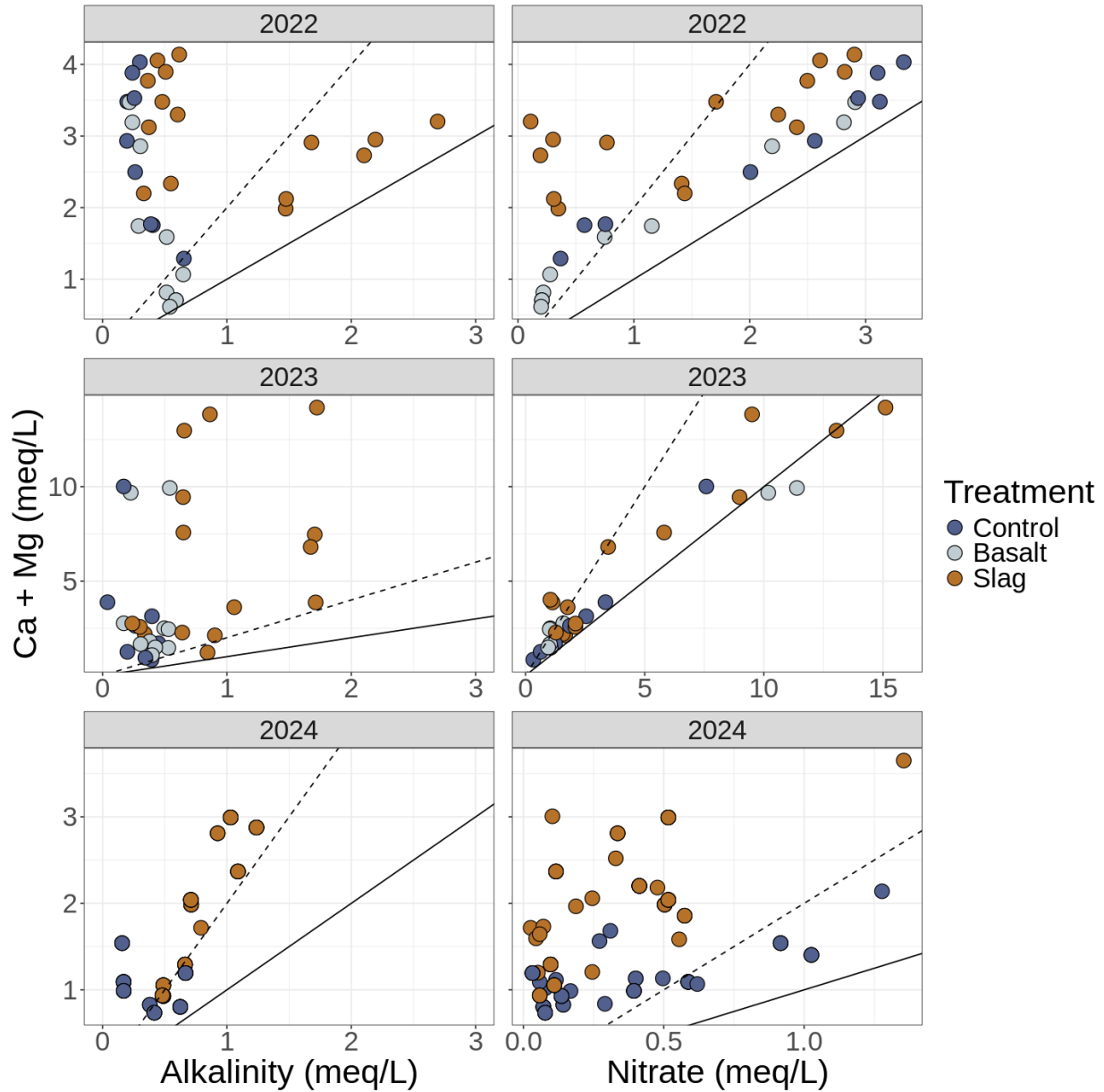


**Figure 5.** Porewater alkalinity (left panel set) and nitrate (right panel set) against base cations calcium and magnesium for each year of field trial monitoring for acidic soils only (. Solid lines represent a 1:1 relationship expected in the case of pure weathering with carbonic acid (alkalinity plots) and nitric acid (nitrate plots). Dashed lines represent 2:1 relationship expected with a mixed carbonic strong acid weathering<sup>43</sup>. Soybeans were planted in 2022 and 2024, which do not require direct fertilization with N-based fertilizers. Corn was planted in 2023 and N-based fertilizers were applied.

Alkalinity loss ( $\Delta\text{HCO}_3^-$ ) is defined as the reduction in alkalinity due to the charge balance of base cations with strong acid anions rather than bicarbonate<sup>52</sup>. Assuming titrated alkalinity is equivalent to the concentration of  $\text{HCO}_3^-$  (in units of  $\text{meq L}^{-1}$ ;

referred to below as  $\text{HCO}_3^-$  measured). The theoretical concentration of  $\text{HCO}_3^-$  ( $\text{HCO}_3^-$  theoretical) is assumed to be equal to the concentration of Ca and Mg (in units of meq  $\text{L}^{-1}$ ) and  $\Delta\text{HCO}_3^-$  is calculated as:

$$\Delta\text{HCO}_3^- = \text{HCO}_3^- \text{theoretical} - \text{HCO}_3^- \text{measured} \quad (\text{eq. 7})$$

Comparison of alkalinity loss to nitrate concentrations reveals a strong linear relationship that is close to a 1:1 line (see Figure 6), suggesting that N-fertilizers are dominantly responsible for alkalinity losses. The observation of this correlation in controls, as well as treated soils, highlights that acid addition in many soils likely leads to alkalinity loss as bicarbonate neutralizes acidity.

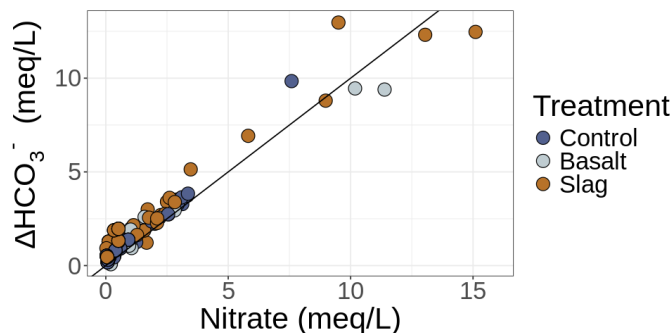


**Figure 6.** Alkalinity loss ( $\Delta\text{HCO}_3^-$ ) plotted against porewater nitrate across all years of the study. The solid line represents a 1:1 ratio showing strong association of nitrate with alkalinity loss.

In acidic soils with low pH, the use of silicate minerals to buffer acidity and bring soils back towards neutral would be particularly attractive relative to carbonate rocks as there would be no risk of releasing fossil  $\text{CO}_2$  from carbonates during neutralization.

The weathering of silicate minerals with strong acids does not lead to a direct removal of  $\text{CO}_2$  and subsequent formation of bicarbonate. However, the buffering effect of a silicate mineral on strong acids like nitric acid should decrease  $\text{CO}_2$  evasion due to acidification and help to retain bicarbonate alkalinity. For instance, consider the carbonate system present in soils (eq. 8):



The net effect of acidification due to nitrogen fertilizers would be to add  $\text{H}^+$ , pushing the equilibrium towards  $\text{CO}_2$  (eq. 8). From a purely inorganic carbon perspective then, acidified systems will degas  $\text{CO}_2$ . Buffering acidity ( $\text{H}^+$ ) from any source of acid (carbonic acid or, in this case, nitric acid) should limit  $\text{CO}_2$  degassing and drive the carbonate system towards bicarbonate thereby encouraging the stability and preservation of alkalinity. The results here support the inclusion of robust

accounting for strong acid weathering and acid neutralization in frameworks for greenhouse gas accounting for enhanced weathering deployments.

## 5. Conclusion

Our three-year field trial of enhanced weathering in the Midwestern U.S. provides evidence that steel slag can deliver measurable carbon dioxide removal (CDR) in acidic soils (initial pH < 6.8) with no carbonate mineral contents. In these settings, steel slag amendments raised soil pH and Ca saturation and elevated soil porewater pH and alkalinity indicating effective weathering leading to CDR at modest application rates (2 tonnes acre<sup>-1</sup>). In contrast, no CDR or weathering signal was detected from basalt amendments, even at higher application rates (10 tonnes acre<sup>-1</sup>), or from steel slag in soils with neutral pH (~7) and pre-existing soil carbonate minerals.

Strong acid driven weathering and/or re-equilibration of the carbonic acid system, primarily from N-fertilizers, was apparent in porewater chemistry during the entire three-year period of monitoring. Strong acid production drives alkalinity loss and blocks the initial removal of CO<sub>2</sub> to bicarbonate. But, buffering acid likely has downstream impacts on the carbonate system that eventually leads to alkalinity preservation (reduced CO<sub>2</sub> degassing), an effect that will likely be difficult to measure.

Measurement techniques for enhanced weathering require high temporal and spatial resolution to detect a relatively small signal in an otherwise noisy system. For porewater chemistry, the dataset presented here was limited due to the labor-intensive nature of sampling and the limited capacity for water recovery in non-saturated media. Soil sampling densities required to detect significant effects were greater than originally anticipated and could indicate substantial time and cost to apply at larger deployment scales. For the measurement techniques that failed to detect a significant signal (chamber-based gas flux measurement and cation-loss mass balance approaches), density of sampling and measurement arrays likely limited the utility of these approaches in this study.

Enhanced weathering continues to emerge as a promising pathway for CDR, but it is critical to better constrain CDR efficiencies in field trials where variable feedstocks are tested in combination with differing soil types and climates. This study provided clear documentation that not all commercially available feedstocks are suitable for deployments. In addition, continued development of sampling and measurement strategies that robustly detect weathering, quantify CDR to develop scalable strategies for monitoring, reporting, and verification are key as enhanced weathering become more widespread.

**Acknowledgements:**

The authors thank several individuals who have contributed to this project, including Adele Fredericks, Demetrius Blackmon-Jimenez, Sebastian Forero Escovar, Jingwen (Crystal) Wu, Anna Greenlee, Ella Cunningham, Fiona Anstey, Sarah Leibovitz, Sophie Naylor, Mike and Shane Peterson, Jonathon Cooper, and Kenzo Esquivel. Funding for this project was provided by Carleton College, the Keck Geology Consortium, and the National Science Foundation under Grant Nos. 2050697 and 2208133. Work at LLNL by NWS was funded by the LLNL LDRD Program (22-LW-022; 24-SI-002) and supported by LLNL’s ‘Terraforming Soil’ Energy Earthshot Research Center (EERC), funded by the U.S. Department of Energy Office of Science, Award# SCW1841, and was performed under the auspices of the DOE, Contract DE-AC52-07NA27344. DPM acknowledges that he is a co-founder of Alkali Earth, a carbon removal startup. Alkali Earth does not deploy or pursue projects related to enhanced weathering on managed croplands.

**Data Availability:**

A full dataset that includes all project data is included as a supplement to this paper and is archived on the CDRXIV repository.

**References:**

- (1) Beerling, D. J.; Kantzas, E. P.; Lomas, M. R.; Taylor, L. L.; Zhang, S.; Kanzaki, Y.; Eufrazio, R. M.; Renforth, P.; Mecure, J.-F.; Pollitt, H.; Holden, P. B.; Edwards, N. R.; Koh, L.; Epihov, D. Z.; Wolf, A.; Hansen, J. E.; Banwart, S. A.; Pidgeon, N. F.; Reinhard, C. T.; Planavsky, N. J.; Val Martin, M. Transforming US Agriculture for Carbon Removal with Enhanced Weathering. *Nature* **2025**, 1–10. <https://doi.org/10.1038/s41586-024-08429-2>.
- (2) Goll, D. S.; Ciais, P.; Amann, T.; Buermann, W.; Chang, J.; Eker, S.; Hartmann, J.; Janssens, I.; Li, W.; Obersteiner, M.; Penuelas, J.; Tanaka, K.; Vicca, S. Potential CO<sub>2</sub> Removal from Enhanced Weathering by Ecosystem Responses to Powdered Rock. *Nat. Geosci.* **2021**, *14* (8), 545–549. <https://doi.org/10.1038/s41561-021-00798-x>.
- (3) Smith, S.; Geden, O.; Gidden, M. J.; Lamb, W. F.; Nemet, G. F.; Minx, J. C.; Buck, H.; Burke, J.; Cox, E.; Edwards, M. R.; Fuss, S.; Johnstone, I.; Müller-Hansen, F.; Pongratz, J.; Probst, B. S.; Roe, S.; Schenuit, F.; Schulte, I.; Vaughan, N. E. The State of Carbon Dioxide Removal 2024 - 2nd Edition., 2024. DOI 10.17605/OSF.IO/F85QJ.
- (4) Seifritz, W. CO<sub>2</sub> Disposal by Means of Silicates. *Nature* **1990**, *345* (6275), 486–486. <https://doi.org/10.1038/345486b0>.
- (5) Hartmann, J.; Kempe, S. What Is the Maximum Potential for CO<sub>2</sub> Sequestration by “Stimulated” Weathering on the Global Scale? *Naturwissenschaften* **2008**, *95* (12), 1159–1164. <https://doi.org/10.1007/s00114-008-0434-4>.

- (6) Köhler, P.; Hartmann, J.; Wolf-Gladrow, D. A. Geoengineering Potential of Artificially Enhanced Silicate Weathering of Olivine. *Proc. Natl. Acad. Sci. U.S.A.* **2010**, *107* (47), 20228–20233. <https://doi.org/10.1073/pnas.1000545107>.
- (7) Hartmann, J.; West, A. J.; Renforth, P.; Köhler, P.; De La Rocha, C. L.; Wolf-Gladrow, D. A.; Dürr, H. H.; Scheffran, J. Enhanced Chemical Weathering as a Geoengineering Strategy to Reduce Atmospheric Carbon Dioxide, Supply Nutrients, and Mitigate Ocean Acidification. *Reviews of Geophysics* **2013**, *51* (2), 113–149. <https://doi.org/10.1002/rog.20004>.
- (8) Beerling, D. J.; Leake, J. R.; Long, S. P.; Scholes, J. D.; Ton, J.; Nelson, P. N.; Bird, M.; Kantzas, E.; Taylor, L. L.; Sarkar, B.; Kelland, M.; DeLucia, E.; Kantola, I.; Müller, C.; Rau, G.; Hansen, J. Farming with Crops and Rocks to Address Global Climate, Food and Soil Security. *Nature Plants* **2018**, *4* (3), 138–147. <https://doi.org/10.1038/s41477-018-0108-y>.
- (9) Beerling, D. J.; Epihov, D. Z.; Kantola, I. B.; Masters, M. D.; Reershemius, T.; Planavsky, N. J.; Reinhard, C. T.; Jordan, J. S.; Thorne, S. J.; Weber, J.; Val Martin, M.; Freckleton, R. P.; Hartley, S. E.; James, R. H.; Pearce, C. R.; DeLucia, E. H.; Banwart, S. A. Enhanced Weathering in the US Corn Belt Delivers Carbon Removal with Agronomic Benefits. *Proc Natl Acad Sci U S A* **2024**, *121* (9), e2319436121. <https://doi.org/10.1073/pnas.2319436121>.
- (10) Kantola, I. B.; Blanc-Betes, E.; Masters, M. D.; Chang, E.; Marklein, A.; Moore, C. E.; von Haden, A.; Bernacchi, C. J.; Wolf, A.; Epihov, D. Z.; Beerling, D. J.; DeLucia, E. H. Improved Net Carbon Budgets in the US Midwest through Direct Measured Impacts of Enhanced Weathering. *Global Change Biology* **2023**, *29* (24), 7012–7028. <https://doi.org/10.1111/gcb.16903>.
- (11) Skov, K.; Wardman, J.; Healey, M.; McBride, A.; Bierowiec, T.; Cooper, J.; Edeh, I.; George, D.; Kelland, M. E.; Mann, J.; Manning, D.; Murphy, M. J.; Pape, R.; Teh, Y. A.; Turner, W.; Wade, P.; Liu, X. Initial Agronomic Benefits of Enhanced Weathering Using Basalt: A Study of Spring Oat in a Temperate Climate. *PLOS ONE* **2024**, *19* (3), e0295031. <https://doi.org/10.1371/journal.pone.0295031>.
- (12) Haque, F.; Santos, R. M.; Dutta, A.; Thimmanagari, M.; Chiang, Y. W. Co-Benefits of Wollastonite Weathering in Agriculture: CO<sub>2</sub> Sequestration and Promoted Plant Growth. *ACS Omega* **2019**, *4* (1), 1425–1433. <https://doi.org/10.1021/acsomega.8b02477>.
- (13) Edwards, D. P.; Lim, F.; James, R. H.; Pearce, C. R.; Scholes, J.; Freckleton, R. P.; Beerling, D. J. Climate Change Mitigation: Potential Benefits and Pitfalls of Enhanced Rock Weathering in Tropical Agriculture. *Biology Letters* **2017**, *13* (4), 20160715. <https://doi.org/10.1098/rsbl.2016.0715>.
- (14) Chiaravalloti, I.; Theunissen, N.; Zhang, S.; Wang, J.; Sun, F.; Ahmed, A. A.; Pihlap, E.; Reinhard, C. T.; Planavsky, N. J. Mitigation of Soil Nitrous Oxide Emissions during Maize Production with Basalt Amendments. *Front. Clim.* **2023**, *5*. <https://doi.org/10.3389/fclim.2023.1203043>.
- (15) Das, S.; Galgo, S. J.; Alam, M. A.; Lee, J. G.; Hwang, H. Y.; Lee, C. H.; Kim, P. J. Recycling of Ferrous Slag in Agriculture: Potentials and Challenges. *Critical*

- Reviews in Environmental Science and Technology* **2020**, *0* (0), 1–35.  
<https://doi.org/10.1080/10643389.2020.1853458>.
- (16) Das, S.; Kim, G. W.; Hwang, H. Y.; Verma, P. P.; Kim, P. J. Cropping With Slag to Address Soil, Environment, and Food Security. *Frontiers in Microbiology* **2019**, *10*, 1320. <https://doi.org/10.3389/fmicb.2019.01320>.
- (17) McDermott, F.; Bryson, M.; Magee, R.; Van Acken, D. Enhanced Weathering for CO<sub>2</sub> Removal Using Carbonate-Rich Crushed Returned Concrete; a Pilot Study from SE Ireland. *Applied Geochemistry* **2024**, *169*, 106056. <https://doi.org/10.1016/j.apgeochem.2024.106056>.
- (18) Clarkson, M. O.; Larkin, C. S.; Swoboda, P.; Reershemius, T.; Suhrhoff, T. J.; Maesano, C. N.; Campbell, J. S. A Review of Measurement for Quantification of Carbon Dioxide Removal by Enhanced Weathering in Soil. *Front. Clim.* **2024**, *6*. <https://doi.org/10.3389/fclim.2024.1345224>.
- (19) Almaraz, M.; Bingham, N. L.; Holzer, I. O.; Geoghegan, E. K.; Goertzen, H.; Sohng, J.; Houlton, B. Z. Methods for Determining the CO<sub>2</sub> Removal Capacity of Enhanced Weathering in Agronomic Settings. *Front. Clim.* **2022**, *4*. <https://doi.org/10.3389/fclim.2022.970429>.
- (20) *Does enhanced weathering work? We're still learning.* – *CarbonPlan*. <https://carbonplan.org/research/enhanced-weathering-fluxes> (accessed 2025-05-14).
- (21) Larkin, C. S.; Andrews, M. G.; Pearce, C. R.; Yeong, K. L.; Beerling, D. J.; Bellamy, J.; Benedick, S.; Freckleton, R. P.; Goring-Harford, H.; Sadekar, S.; James, R. H. Quantification of CO<sub>2</sub> Removal in a Large-Scale Enhanced Weathering Field Trial on an Oil Palm Plantation in Sabah, Malaysia. *Front. Clim.* **2022**, *4*. <https://doi.org/10.3389/fclim.2022.959229>.
- (22) Gunnarsen, K. C.; Schjoerring, J. K.; Gómez-Muñoz, B.; de Neergaard, A.; Jensen, L. S. Can Silicon in Glacial Rock Flour Enhance Phosphorus Availability in Acidic Tropical Soil? *Plant Soil* **2022**, *477* (1), 241–258. <https://doi.org/10.1007/s11104-022-05399-0>.
- (23) Guo, F.; Wang, Y.; Zhu, H.; Zhang, C.; Sun, H.; Fang, Z.; Yang, J.; Zhang, L.; Mu, Y.; Man, Y. B.; Wu, F. Crop Productivity and Soil Inorganic Carbon Change Mediated by Enhanced Rock Weathering in Farmland: A Comparative Field Analysis of Multi-Agroclimatic Regions in Central China. *Agricultural Systems* **2023**, *210*, 103691. <https://doi.org/10.1016/j.agsy.2023.103691>.
- (24) Holzer, I. O.; Nocco, M. A.; Houlton, B. Z. Direct Evidence for Atmospheric Carbon Dioxide Removal via Enhanced Weathering in Cropland Soil. *Environ. Res. Commun.* **2023**, *5* (10), 101004. <https://doi.org/10.1088/2515-7620/acfd89>.
- (25) Reershemius, T.; Kelland, M. E.; Jordan, J. S.; Davis, I. R.; D'Ascanio, R.; Kalderon-Asael, B.; Asael, D.; Suhrhoff, T. J.; Epihov, D. Z.; Beerling, D. J.; Reinhard, C. T.; Planavsky, N. J. Initial Validation of a Soil-Based Mass-Balance Approach for Empirical Monitoring of Enhanced Rock Weathering Rates. *Environ. Sci. Technol.* **2023**, *57* (48), 19497–19507. <https://doi.org/10.1021/acs.est.3c03609>.

- (26) Suhrhoff, T. J.; Reershemius, T.; Wang, J.; Jordan, J. S.; Reinhard, C. T.; Planavsky, N. J. A Tool for Assessing the Sensitivity of Soil-Based Approaches for Quantifying Enhanced Weathering: A US Case Study. *Front. Clim.* **2024**, *6*. <https://doi.org/10.3389/fclim.2024.1346117>.
- (27) McBride, A. L.; Skov, K.; Wade, P.; Betz, J.; Stubbs, A.; Albahri, T.; Cazzagon, G.; Chen, C.-J.; Frew, A.; Idam, I.; Jones, L.; Kelland, M. E.; Mann, J.; Manning, D.; Murphy, M. J.; Radkova, A.; Teh, Y. A.; Tostevin, R.; Turner, W.; Wardman, J.; Wilkie, M.; Liu, X. Quantifying Potential Carbon Dioxide Removal via Enhanced Weathering Using Porewater from a Field Trial in Scotland. *EarthArXIV* **2025**, *Pre-Print*. <https://doi.org/10.31223/X5NX5H>.
- (28) Taylor, L. L.; Driscoll, C. T.; Groffman, P. M.; Rau, G. H.; Blum, J. D.; Beerling, D. J. Increased Carbon Capture by a Silicate-Treated Forested Watershed Affected by Acid Deposition. *Biogeosciences* **2021**, *18* (1), 169–188. <https://doi.org/10.5194/bg-18-169-2021>.
- (29) Neal, C. Alkalinity Measurements within Natural Waters: Towards a Standardised Approach. *Science of The Total Environment* **2001**, *265* (1–3), 99–113. [https://doi.org/10.1016/S0048-9697\(00\)00652-5](https://doi.org/10.1016/S0048-9697(00)00652-5).
- (30) Slessarev, E. W.; Chadwick, O. A.; Sokol, N. W.; Nuccio, E. E.; Pett-Ridge, J. Rock Weathering Controls the Potential for Soil Carbon Storage at a Continental Scale. *Biogeochemistry* **2021**. <https://doi.org/10.1007/s10533-021-00859-8>.
- (31) Kanzaki, Y.; Planavsky, N.; Zhang, S.; Jordan, J.; Suhrhoff, T. J.; Reinhard, C. T. Soil Cation Storage as a Key Control on the Timescales of Carbon Dioxide Removal through Enhanced Weathering.
- (32) Power, I. M.; Hatten, V. N. J.; Guo, M.; Schaffer, Z. R.; Rausis, K.; Klyn-Hesselink, H. Are Enhanced Rock Weathering Rates Overestimated? A Few Geochemical and Mineralogical Pitfalls. *Front. Clim.* **2025**, *6*, 1510747. <https://doi.org/10.3389/fclim.2024.1510747>.
- (33) Scharlemann, J. P.; Tanner, E. V.; Hiederer, R.; Kapos, V. Global Soil Carbon: Understanding and Managing the Largest Terrestrial Carbon Pool. *Carbon Management* **2014**, *5* (1), 81–91. <https://doi.org/10.4155/cmt.13.77>.
- (34) Sokol, N. W.; Sohng, J.; Moreland, K.; Slessarev, E.; Goertzen, H.; Schmidt, R.; Samaddar, S.; Holzer, I.; Almaraz, M.; Geoghegan, E.; Houlton, B.; Montañez, I.; Pett-Ridge, J.; Scow, K. Reduced Accrual of Mineral-Associated Organic Matter after Two Years of Enhanced Rock Weathering in Cropland Soils, Though No Net Losses of Soil Organic Carbon. *Biogeochemistry* **2024**, *167* (8), 989–1005. <https://doi.org/10.1007/s10533-024-01160-0>.
- (35) Xu, T.; Yuan, Z.; Vicca, S.; Goll, D. S.; Li, G.; Lin, L.; Chen, H.; Bi, B.; Chen, Q.; Li, C.; Wang, X.; Wang, C.; Hao, Z.; Fang, Y.; Beerling, D. J. Enhanced Silicate Weathering Accelerates Forest Carbon Sequestration by Stimulating the Soil Mineral Carbon Pump. *Global Change Biology* **2024**, *30* (8), e17464. <https://doi.org/10.1111/gcb.17464>.
- (36) Buss, W.; Hasemer, H.; Sokol, N. W.; Rohling, E. J.; Borevitz, J. Applying Minerals to Soil to Draw down Atmospheric Carbon Dioxide through

- Synergistic Organic and Inorganic Pathways. *Commun Earth Environ* **2024**, *5* (1), 602. <https://doi.org/10.1038/s43247-024-01771-3>.
- (37) Soil Survey Staff, N. R. C. S., United States Department of Agriculture. *Web Soil Survey - Home*. <https://websoilsurvey.nrcs.usda.gov/app/homepage.htm> (accessed 2025-05-20).
- (38) Wirth, K. R.; Naiman, Z. J.; Vervoort, J. D. The Chengwatana Volcanics, Wisconsin and Minnesota: Petrogenesis of the Southernmost Volcanic Rocks Exposed in the Midcontinent Rift. *Can. J. Earth Sci.* **1997**, *34* (4), 536–548. <https://doi.org/10.1139/e17-043>.
- (39) Sokol, N. W.; Kuebbing, S. E.; Bradford, M. A. Impacts of an Invasive Plant Are Fundamentally Altered by a Co-occurring Forest Disturbance. *Ecology* **2017**, *98* (8), 2133–2144. <https://doi.org/10.1002/ecy.1906>.
- (40) Bradford, M. A.; Fierer, N.; Reynolds, J. F. Soil Carbon Stocks in Experimental Mesocosms Are Dependent on the Rate of Labile Carbon, Nitrogen and Phosphorus Inputs to Soils. *Functional Ecology* **2008**, *22* (6), 964–974. <https://doi.org/10.1111/j.1365-2435.2008.01404.x>.
- (41) PP Systems. EGM-5 Portable CO<sub>2</sub> Gas Analyzer Operations Manual Version 1.03, 2018.
- (42) O'Connor, J.; Nguyen, T. B. T.; Honeyands, T.; Monaghan, B.; O'Dea, D.; Rinklebe, J.; Vinu, A.; Hoang, S. A.; Singh, G.; Kirkham, M. B.; Bolan, N. Production, Characterisation, Utilisation, and Beneficial Soil Application of Steel Slag: A Review. *Journal of Hazardous Materials* **2021**, *419*, 126478. <https://doi.org/10.1016/j.jhazmat.2021.126478>.
- (43) Hamilton, S. K.; Kurzman, A. L.; Arango, C.; Jin, L.; Robertson, G. P. Evidence for Carbon Sequestration by Agricultural Liming. *Global Biogeochemical Cycles* **2007**, *21* (2). <https://doi.org/10.1029/2006GB002738>.
- (44) Oh, N.; Raymond, P. A. Contribution of Agricultural Liming to Riverine Bicarbonate Export and CO<sub>2</sub> Sequestration in the Ohio River Basin. *Global Biogeochemical Cycles* **2006**, *20* (3), 2005GB002565. <https://doi.org/10.1029/2005GB002565>.
- (45) Kang, J.; Qu, C.; Chen, W.; Cai, P.; Chen, C.; Huang, Q. Organo–Organic Interactions Dominantly Drive Soil Organic Carbon Accrual. *Global Change Biology* **2024**, *30* (1), e17147. <https://doi.org/10.1111/gcb.17147>.
- (46) Rowley, M. C.; Grand, S.; Verrecchia, É. P. Calcium-Mediated Stabilisation of Soil Organic Carbon. *Biogeochemistry* **2018**, *137* (1–2), 27–49. <https://doi.org/10.1007/s10533-017-0410-1>.
- (47) Shabtai, I. A.; Wilhelm, R. C.; Schweizer, S. A.; Höschen, C.; Buckley, D. H.; Lehmann, J. Calcium Promotes Persistent Soil Organic Matter by Altering Microbial Transformation of Plant Litter. *Nat Commun* **2023**, *14* (1), 6609. <https://doi.org/10.1038/s41467-023-42291-6>.
- (48) King, A. Soil Carbon Formation Is Promoted by Saturation Deficit and Existing Mineral-Associated Carbon, Not by Microbial Carbon-Use Efficiency. *Science Advances* **2025**, *11*, eadv9482. <https://doi.org/DOI: 10.1126/sciadv.adv9482>.

- (49) Malik, A. A.; Puissant, J.; Buckeridge, K. M.; Goodall, T.; Jehmlich, N.; Chowdhury, S.; Gweon, H. S.; Peyton, J. M.; Mason, K. E.; Van Agtmaal, M.; Blaud, A.; Clark, I. M.; Whitaker, J.; Pywell, R. F.; Ostle, N.; Gleixner, G.; Griffiths, R. I. Land Use Driven Change in Soil pH Affects Microbial Carbon Cycling Processes. *Nat Commun* **2018**, *9* (1), 3591.  
<https://doi.org/10.1038/s41467-018-05980-1>.
- (50) Vermeiren, C.; Ceulemans, J.; Thiry, Y.; Smolders, E. Increased Soil pH and Enhanced Microbial Activity Stimulate the Gradual Immobilisation of Selenate Added to Soils. *Soil Biology and Biochemistry* **2025**, *202*, 109688.  
<https://doi.org/10.1016/j.soilbio.2024.109688>.
- (51) Fernández-Calviño, D.; Bååth, E. Growth Response of the Bacterial Community to pH in Soils Differing in pH: Growth Response of the Bacterial Community to pH. *FEMS Microbiology Ecology* **2010**, no-no.  
<https://doi.org/10.1111/j.1574-6941.2010.00873.x>.
- (52) Milliken, E.; Woodley, A.; Planavsky, N. Direct Measurement of Carbon Dioxide Removal Due to Enhanced Weathering. CDRXIV 2025.  
<https://doi.org/10.70212/cdrxiv.2025352.v1>.
- (53) Perrin, A.-S.; Probst, A.; Probst, J.-L. Impact of Nitrogenous Fertilizers on Carbonate Dissolution in Small Agricultural Catchments: Implications for Weathering CO<sub>2</sub> Uptake at Regional and Global Scales. *Geochimica et Cosmochimica Acta* **2008**, *72* (13), 3105–3123.  
<https://doi.org/10.1016/j.gca.2008.04.011>.

## Supplemental Material



**Figure S1.** Historical aerial imagery from 1991-2023 showing land use differences across the field site. White rectangle indicates approximate position of the experimental area used for the field trial. Note the more variable use of the northern position of the field area, except for the Northeast corner. The field site has been in agriculture since the 1930's. Dredged lake sediments were spread on the Northwestern portion of the field at some point in the early 2000's, and the transition from full to strip tillage occurred around 2014.

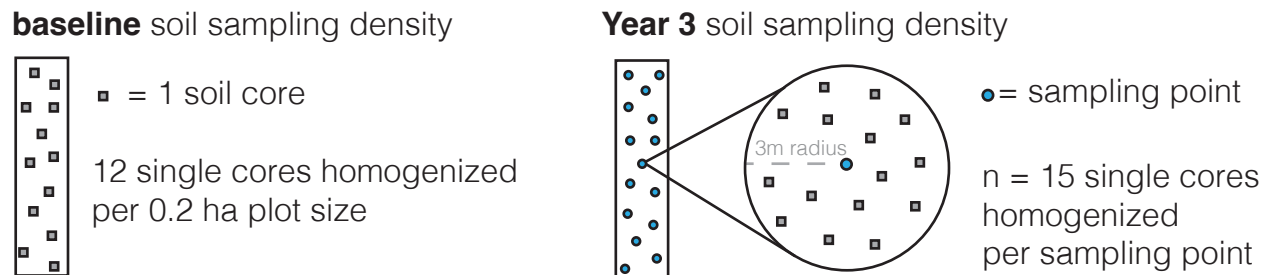


**Figure S2.** Sampling density for soil cores between baseline (left) and year 3 sampling (right). In the baseline style sampling, 12 individual soil cores were collected at each depth interval and homogenized for a single plot sample used for analysis. In contrast, for year 3 style sampling there were 15 sampling points established per plot. At each sampling point, 15 individual soil cores were taken and homogenized for analysis of each individual sampling point. Baseline style sampling was used for baseline soil collection in 2021 and year 1 soils at 0-10 cm and 10-20 cm in 2022. Year 3 style sampling was used for the whole field in 2024 and for the southern blocks (C and D) for year 2 in 2023. Year 3 style sampling was only done for 0-10 cm depth.

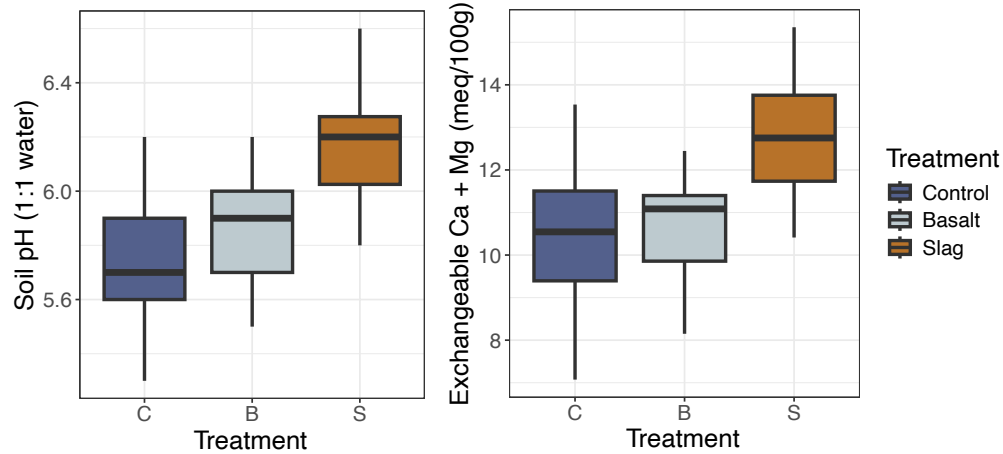


**Figure S3.** Results for soil pH (1:1 water to soil ratio; left panel) and exchangeable calcium and magnesium (right panel) for year 2 soils in the southern blocks C and D sampled at higher density using the sample point sampling strategy (see manuscript, and Figure S3). Note the relatively low soil pH for all soils. There is no statistical difference between control and basalt treatments ( $p = 0.015$ ; Tukey HSD and ANOVA test) for either property shown here, however increases in soil pH and exchangeable Ca and Mg for slag treatments are statistically significant compared against control ( $p < 0.001$ ) and basalt ( $p < 0.001$ ). All box plots include  $n = 15$  sampling points per plot, with two plots per treatment ( $n = 30$  total). Soil sampling depth is 0-10 cm for all samples evaluated here.

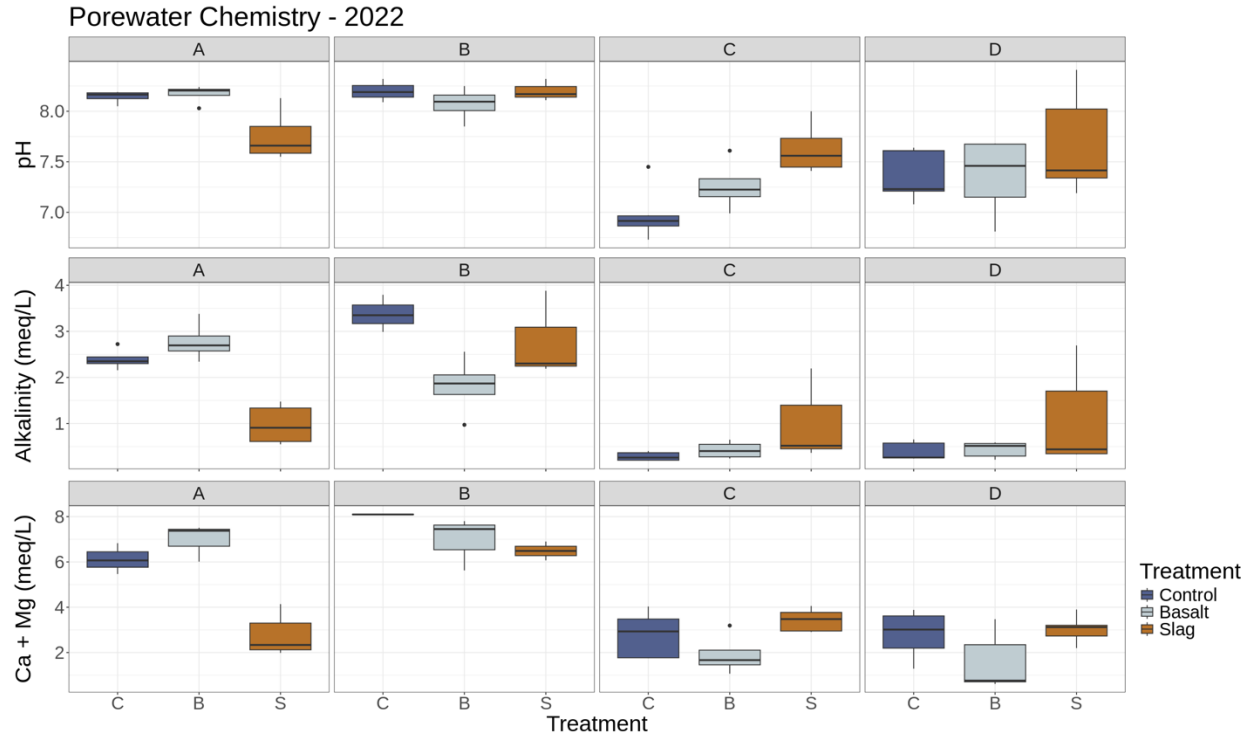


**Figure S4.** Water chemistry across block during the first year of the field trial monitoring in 2022. Note the elevated porewater pH (upper), alkalinity (middle), and Ca and Mg (lower) in block B and the basalt and control plots of block A.

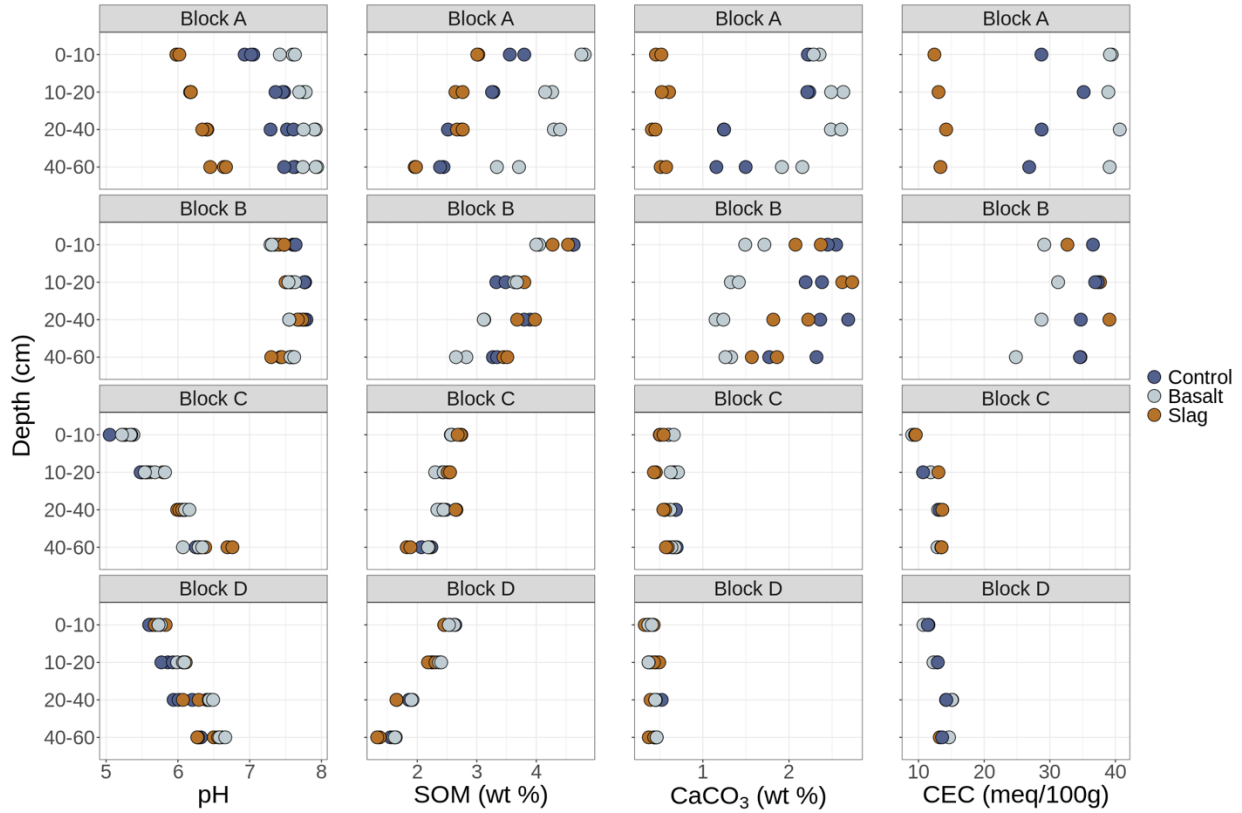


**Figure S5.** Baseline soil properties for pH, soil organic matter (SOM), carbonate (CaCO<sub>3</sub>), and cation exchange capacity (CEC) across blocks (labeled with grey header) and treatment plots (colored symbols). All soil sampled in June 2021 prior to any treatment application. Note that there is a clear distinction between soils in the northern blocks, A and B, compared with southern plots in blocks C and D.

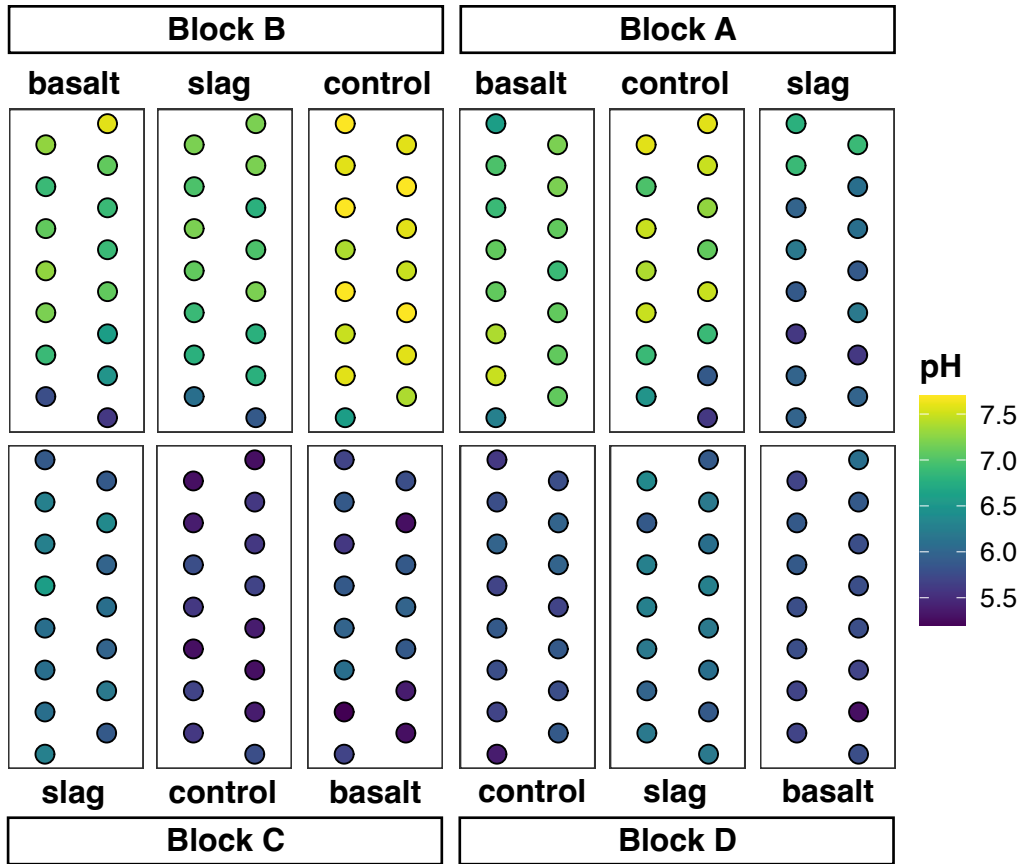


**Figure S6.** Soil pH shown schematically across the study area within each experimental plot for 0-10 cm soil sampled in 2024 (year 3 of study). Individual plots are ~100 x 20 m wide. Each colored circle represents a sampling point with  $n = 15$  individual soil cores composited into a single point sample representing a 3 m radius (see Methods). Note variation across study area and within individual plots.

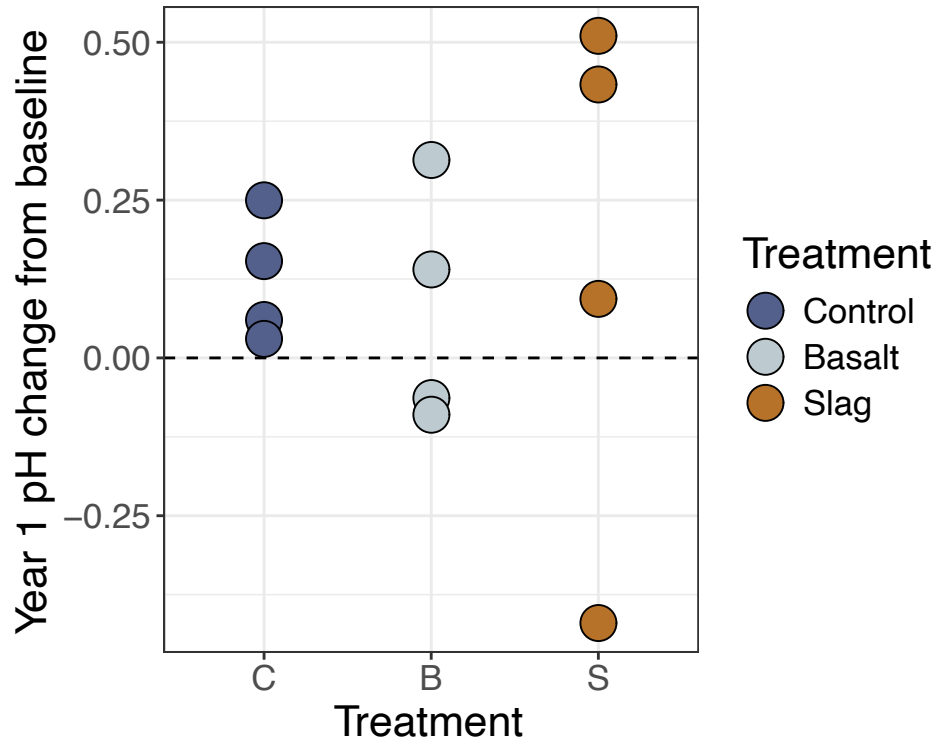


**Figure S7.** Change in soil pH for 0-10 cm depth interval for year 1 (2022) compared to baseline (2021) in all experimental plots. Low density soil sampling could play a role in variable results obtained here.

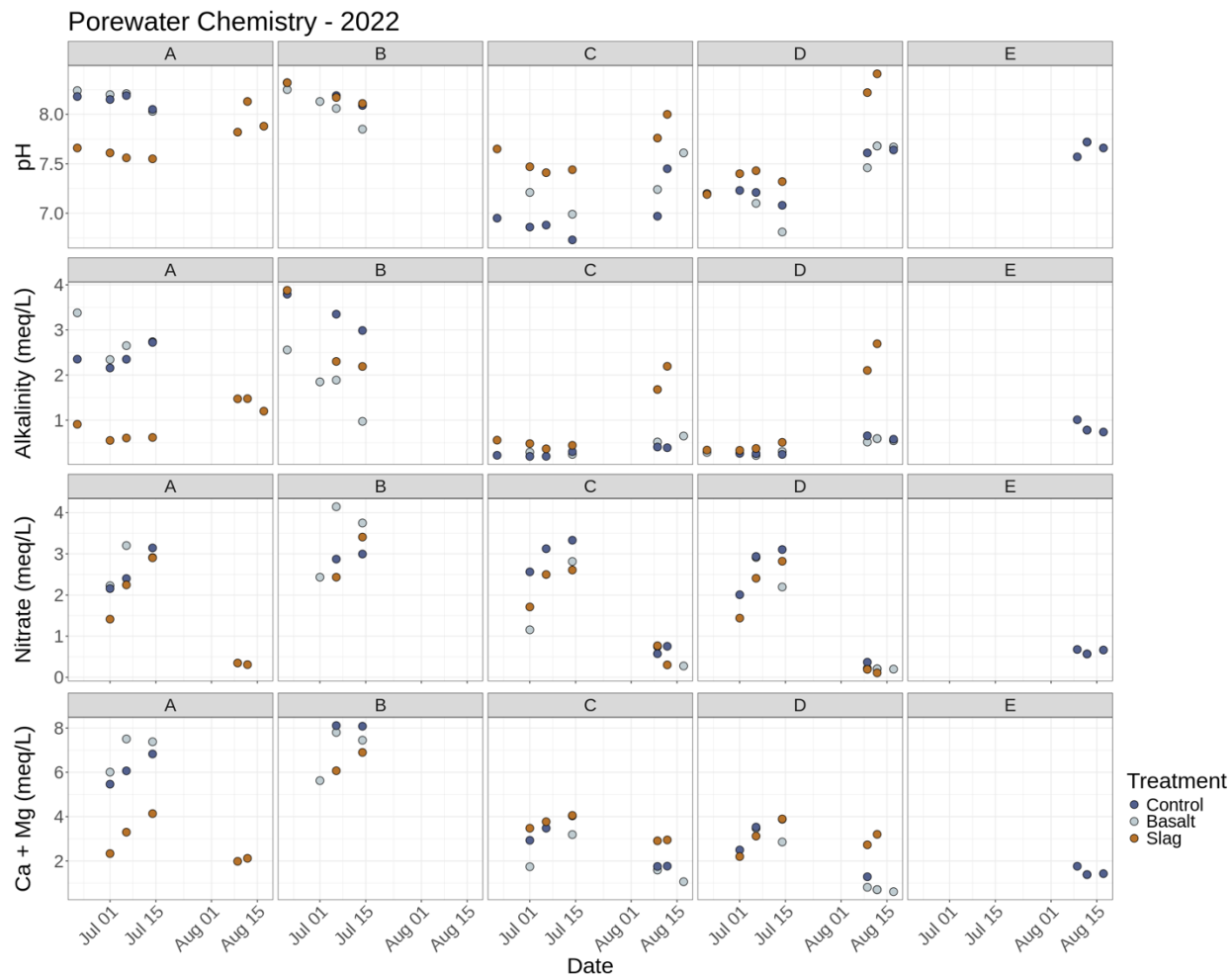


**Figure S8.** Porewater chemistry from year 1 (2022) against sampling date showing temporal variations. Gaps in data collection for blocks C, D, and plot A-slag occur due to dry conditions during late July and early August. Block E sampling began late in the season to serve as additional control (E block lysimeters installed between Blocks C and D in buffer strips – see main text).

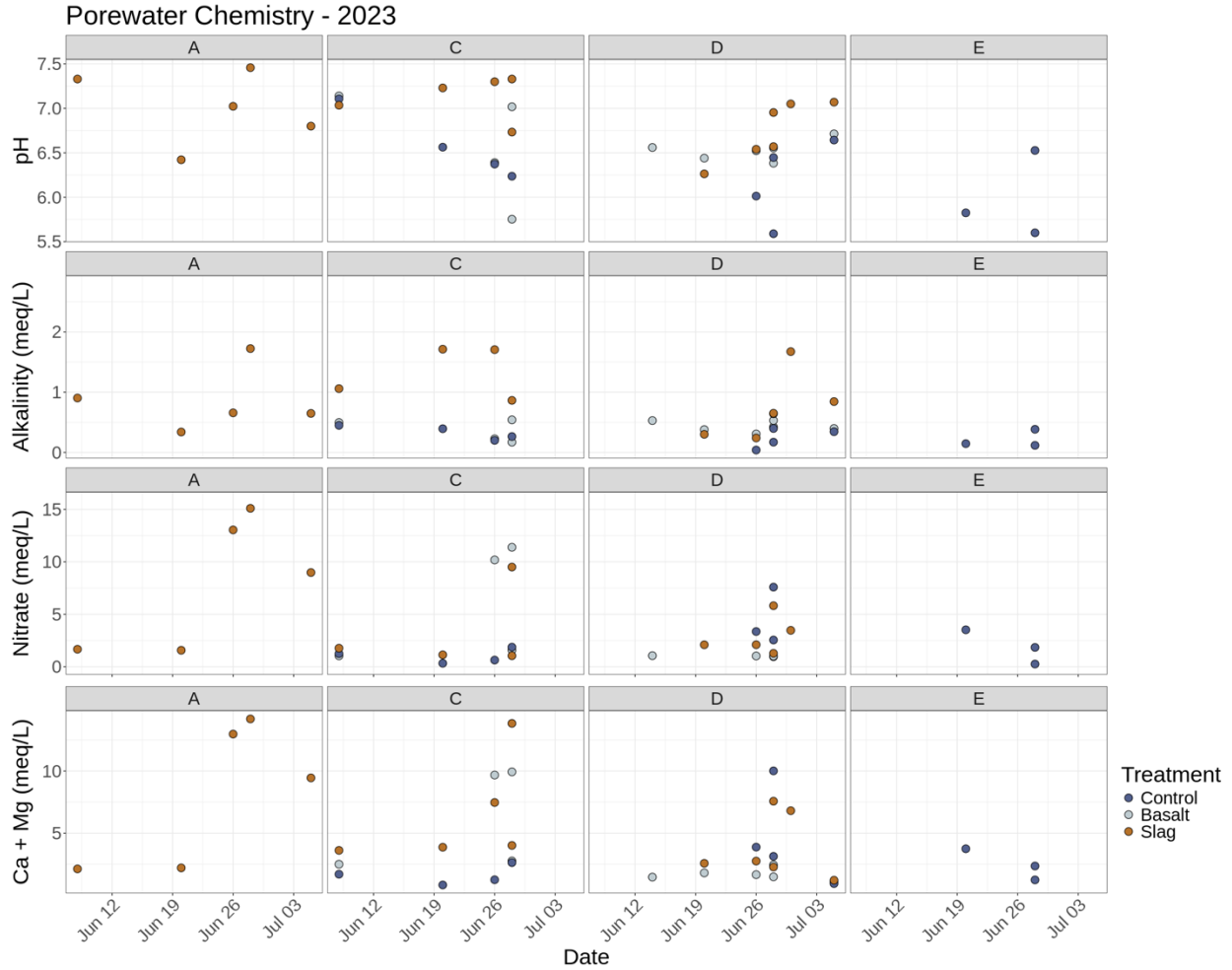


**Figure S9.** Porewater chemistry from year 2 (2023) against sampling date showing temporal variations. Gaps in data collection for blocks C, D, and plot A-slag occur due to dry conditions during late July and early August. Block E lysimeters installed between Blocks C and D in buffer strips – see main text.

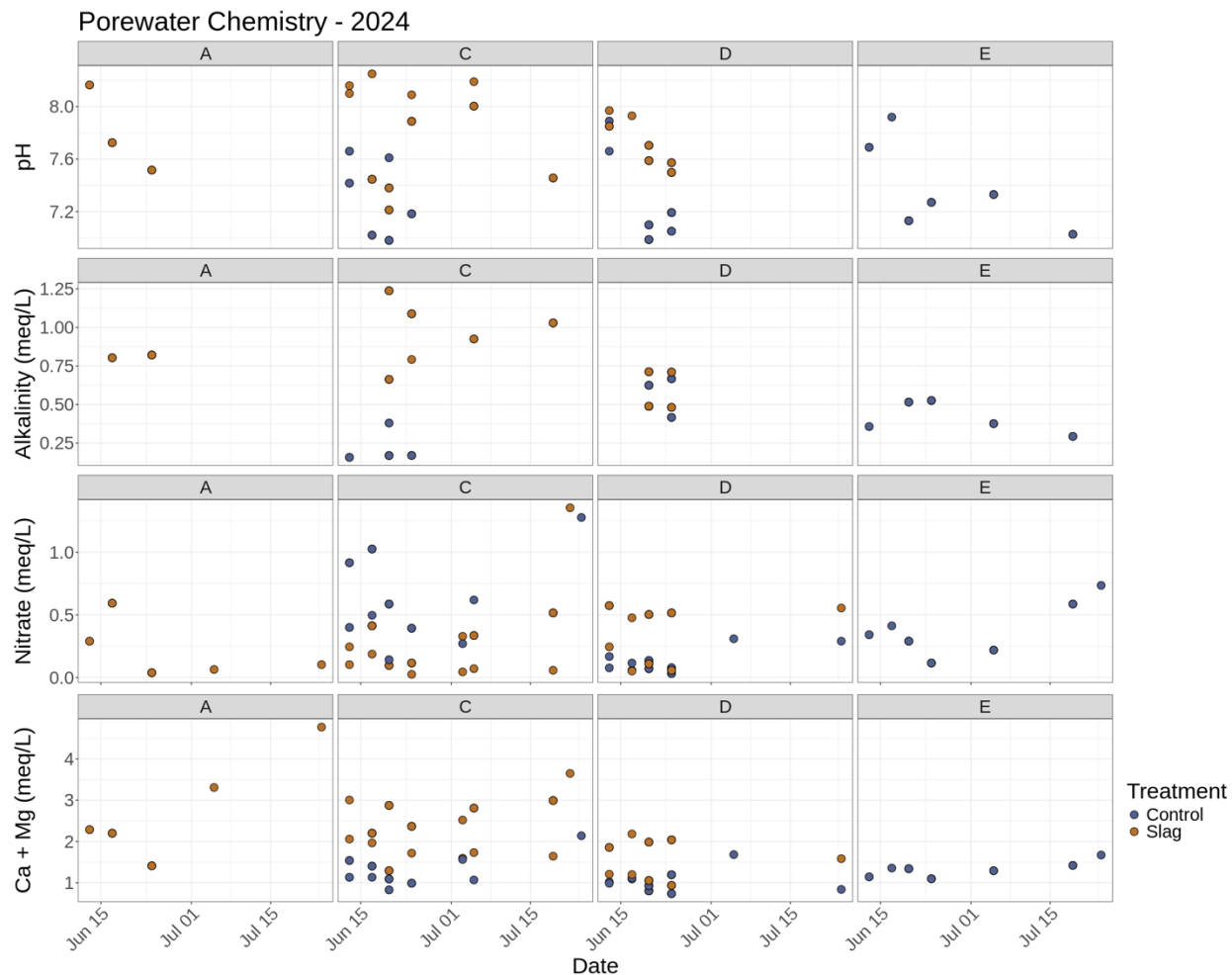


**Figure S10.** Porewater chemistry from year 3 (2024) against sampling date showing temporal variations. Gaps in data collection for blocks C, D, and plot A-slag occur due to dry conditions during late July and early August. Block E lysimeters installed between Blocks C and D in buffer strips – see main text. Note that only slag and control plots monitored during 2024 in an effort to maximize water recovery.

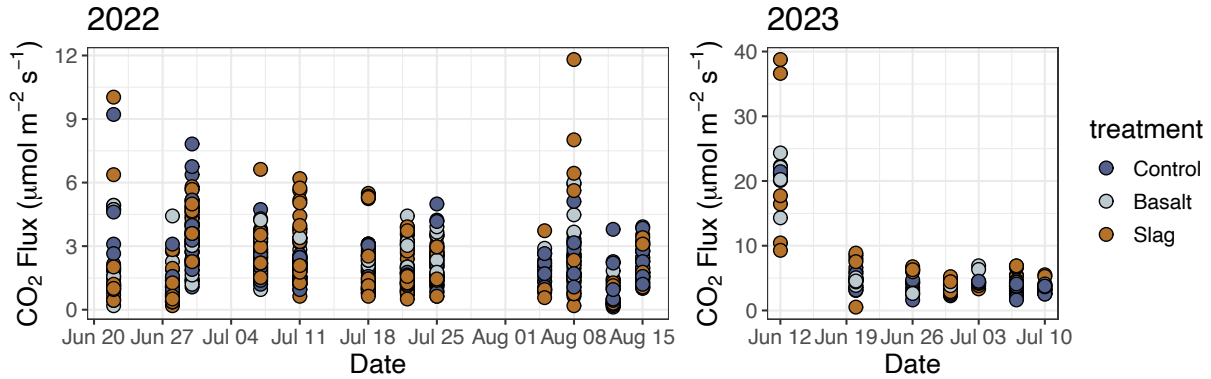


**Figure S11.** CO<sub>2</sub> gas flux data for 2022 and 2023. Variability within any one measurement day was relatively high due to diurnal changes. There is no clear change in CO<sub>2</sub> flux based on basalt or slag treatments across all observed periods in this study.

**Table S1.** Climate and weather data for 1990-2020 annual average and growing season (May-Sept) normal conditions and yearly values for Rice County, Minnesota during the three calendar years of the field trial. All data from NOAA.

	<b>Annual Average</b>	<b>2022</b>	<b>2023</b>	<b>2024</b>
Precipitation (mm)	902	685	822	1003
Temperature (°C)	7.9	6.4	8.5	9.3
	<b>Growing Season</b>	<b>2022</b>	<b>2023</b>	<b>2024</b>
Precipitation (mm)	574	413	373	704
Temperature (°C)	18.5	19.2	20.0	19.3

**Table S2.** Spreading rates calculated from pan tests in the field. Target application rates were 2 and 10 tonnes per acre for slag and basalt, respectively. Application rates for the slag treatment were  $2.06 \pm 0.08$  tonnes acre<sup>-1</sup> (reported error is one standard deviation). Basalt application rates were far more variable, with an average of  $10.09 \pm 3.88$  tonnes acre<sup>-1</sup>.

<b>Treatment</b>	<b>Block</b>	<b>Pan Measured Rate (tonne/acre)</b>
Slag	A	2.0
Slag	B	2.0
Slag	C	2.0
Slag	D	2.2
Basalt	A	11.0
Basalt	B	14.8
Basalt	C	11.1
Basalt	D	7.1